Doctoral Thesis

Restoration of Volitional Motor Control via an Artificial Neural Connection

Kenji KATO

(Student ID: 20112002)

Doctoral adviser: Tadashi ISA

2014 / 3

School of Life Science,

The Graduate University for Advanced Studies (SOKENDAI)

Table of contents

General introduction

It is estimated that over 5,130,000 people over the world each year are attacked by stroke (http://www.world-heart-federation.org/cardiovascular-health/stroke/, 2013) or spinal cord injury (SCI, http://www.campaignforcure.org, 2011) which often lead to paralysis and impairment of their daily living activities. Brain machine interfaces (BMIs) can directly connect the patients' brains to external devices such as the robotic arm, thereby have a possibility to help the patients manage their daily living activities (Carmena et al., 2003; Hochberg et al., 2006; Ganguly et al., 2009; Ganguly et al., 2011; Hochberg et al., 2012). However, what patients really hope for would be to regain their own impaired motor functions. Paralysis following stroke or SCI is mainly attributed to the interruption of descending pathways from the supraspinal motor centers to the spinal motor neurons, although the neural circuits located above and below the lesion sites would remain functional. An artificial neural connection (ANC) is a promising closed-loop neural prosthesis which bridges the damaged neural pathways by artificially reconnecting the preserved neural structures, thereby has a potential to compensate for the functional impairment of the extremities (Moritz et al., 2008; Nishimura et al., 2013a). Basically, ANC is based on the concept of constructing a bridge between two separated neural structures via the computer interface, which can record the neural

activities as the input signal and deliver the activity-contingent electrical stimulation to another neural structures as the output signal with the physiological delay which mimics the conduction delay of the targeted neural pathway (Jackson et al., 2006; Moritz et al., 2008; Lucas et al., 2013; Nishimura et al., 2013a; Nishimura et al., 2013b). However, to achieve the skilled control with ANC, subjects need to learn the causal relationship between input and output signal of ANC. Recent studies have demonstrated that monkeys could learn to use their cortical activity to control functional electrical stimulation of muscles which were transiently paralyzed by nerve block (Moritz et al., 2008; Pohlmeyer et al., 2009; Ethier et al., 2012). However, it remains unclear whether individuals with damaged-brain after stroke have an essential adaptability to control their paretic limb with a novel ANC. And if so, the neural mechanism underlying such adaptation process to ANC is largely unknown.

To answer this, first, in Part I of this thesis, I investigated the effects of introducing an artificial cortico-muscular connection (ACMC) in a paretic monkey that had a unilateral stroke at the corona radiata level, and examined whether monkeys with extensive subcortical damage had an adequate adaptability to control ANC to restore one-dimensional goal-directed movement. The ACMC detects the arbitrary-discriminated high-gamma neural oscillations recorded from motor related

areas as the input signal, and converted in real-time to activity-contingent electrical stimuli delivered to the paretic muscle as the output signal. To further understand the neural mechanism underlying adaptation to ANC, I investigated the learning-related modulation of the input-related activities over large-scale cortical areas.

Second, in Part II of this thesis, for clinical application of ANC into human subjects with non-invasive approach, I developed an artificial recurrent connection (ARC) from muscle activity to peripheral nerve, and confirmed healthy individuals also could be adapted to ARC. In this paradigm, the ulnar nerve was stimulated in proportion to activation of the muscle homonymous or synergistic to those innervated by the nerve, which boosted the on-going activity of the homonymous muscle and wrist movement during the visually-guided reaching task around the wrist. Thus, I investigated the motor adaptation process by evaluating the overreached lengths from the target. To clarify the neurophysiological mechanism of the motor adaptation process, I also investigated the activity of homonymous muscle, their synergist muscle, and antagonist muscle.

I demonstrated that monkeys with stroke as well as healthy individuals could flexibly get adapted to a novel ANC by leaning its causal input-output relationship.

Part I

Title: **Flexible adaptation of extensive cortical area to artificial corticomuscular connection in stroke monkeys**

Abstract

Brain stroke disconnects the brain from the body, eliminating the ability to perform volitional movements. An artificial neural connection which rewires the preserved neural structures beyond damaged sites, might compensate for the paralysis. Here, I demonstrated that the stroke-model monkeys which experienced subcortical damage restored the volitional one-dimensional movement of the paretic hand through the artificial corticomuscular connection (ACMC), by which forearm muscles were electrically stimulated by transforming the neural signal in the sensorimotor cortex. Although the corticofugal fibers and the striatum were extensively damaged, adaptation to ACMC was rapidly induced by modulation of the input signal in the arbitrarily-selected high-gamma band range for ACMC. The input signal was selected from randomly-assigned single electrode in each session, however, the monkeys were flexibly adapted to ACMC using signals from various electrodes placed either in the premotor, primary motor, or primary sensory cortices. Such flexible and rapid adaptation was induced through a large-scaled reorganization of cortical activity in the high-gamma band. During learning, the strongest high-gamma modulation became concentrated on the areas close to the input electrode. These findings indicated that monkeys with extensive subcortical damage had adequate adaptability to control the

closed-loop neuroprosthesis by rapidly reorganizing the input-related cortical activity over large-scaled cortical areas, suggesting that the artificial neural connection is a promising future approach to restore the impaired motor function of paretic extremities in brain injury.

Introduction

Paralysis after stroke is among leading issues for patients with long-term motor impairments and therefore a primary target for the application of brain-machine interfaces (BMIs) (Carmena et al., 2003; Hochberg et al., 2006; Ganguly et al., 2009; Ganguly et al., 2011; Hochberg et al., 2012). BMIs directly connect the patients' brain to external devices, and have a potential to help to manage their daily living activities. However, what patients really hope for would be to regain their own impaired motor functions. The paralysis of limb after stroke is mainly attributed to the interruption of descending pathways from the supraspinal motor centers to the spinal motor neurons. This means that neural structures above and below the lesion sites, in the brain as well as the spinal cord, and muscles would remain functional. An artificial neural connection (ANC) is a promising neural prosthesis which bridges the damaged neural pathways by artificially reconnecting the preserved neural structures, thereby has a possibility to compensate for the functional impairment of their extremities. Recent studies have demonstrated that monkeys could learn to use cortical activity to control functional electrical stimulation (FES) of muscles which were transiently paralyzed by nerve block (Moritz et al., 2008; Pohlmeyer et al., 2009; Ethier et al., 2012), and of the spinal circuits after cervical spinal cord injury (Nishimura et al., 2013a), however, it still

remains unclear whether individuals with damaged brain after stroke has an essential adaptability to control the closed-loop neural prosthesis.

Over the last 50 years, the animal's ability to directly modulate specific neural signal has been demonstrated in subjects with intact brain. When given feedback, the animals can rapidly learn to volitionally control the activity of neurons (Fetz, 1969; Fetz and Baker, 1973; Kennedy and Bakay, 1998; Chapin et al., 1999), population of neuron (Leuthardt et al., 2004; Wolpaw et al., 1991; Fabiani et al., 2004; Miller et al., 2010) during motor execution or motor imagery. Such modulation can be made even when overt movements are impossible in case of individuals with amyotrophic lateral sclerosis (Kennedy and Bakay. 1998) or tetraplegia (Hochberg et al., 2006; Hochberg et al., 2012).

However, to achieve skilled control of neuroprosthesis, various types of learning will be required which include abstract processing like motor planning or imagery, and physical control like playing guitar or riding a bicycle. A large amount of literature suggested the neural circuits and structures involved in these types of learning (Georgopoulos et al., 1993; Fincham et al., 2006; Yin et al., 2009; Kimchi and Laubach, 2009; Badre et al., 2010; Koralek et al., 2012). For example, the cortico-basal ganglia circuits have been implicated in the learning, selection and execution of physical skills

(Yin et al., 2009; Kimchi and Laubach, 2009). On the other hand, the motor cortex and frontal cortices have been implicated in the learning of abstract skills (Georgopoulos et al., 1993; Gandolfo et al., 2000; Fincham et al., 2006; Badre et al., 2010), and in learning to control neuroprosthetic devices irrespective of physical movement (Taylor et al., 2002; Ganguly et al., 2003; Ganguly et al., 2011). Some studies suggest that not only cortical areas, but also the striatum, are necessary for learning intentional skills to control the neuroprosthetic device (Koralek et al., 2012). Therefore, it is important to test whether the subject with large subcortical damage including the striatum and corticofugal fibers could learn to control the neuroprosthetic devices using the animal model with subcortical stroke. Here, I demonstrated that monkeys with chronic paralysis of extremity caused by extensive subcortical stroke at the corona radiate level could adapt to an artificial cortico-muscular connection (ACMC) which uses the neural oscillatory signal recorded from the preserved cortical sensorimotor areas to control electrical stimulation in paretic muscles to restore goal-directed movement of the affected arm. Here, I used arbitrary-discriminated high-gamma neural oscillations recorded from one of the randomly-selected electrodes placed in motor related areas as the input signal for ACMC. I investigated adaptation process to ACMC by calculating the task-related modulation of the input-related activities over large-scaled cortical

areas.

Methods

Experiments were performed with three male Macaca monkeys. (two *Macaca fuscata*; 9.0 kg in monkey M and 7.5 kg in monkey TA. A *Macaca mulatta*; 9.8 kg in monkey TE). All experimental procedures were performed in accordance with the Guidelines for Proper Conduct of Animal Experiments of the Science Council of Japan and approved by the Committee for Animal Experiment at the National Institutes of Natural Sciences.

Surgeries

All implant surgeries were performed using sterile techniques while the animal was anesthetized using 1-2 % isoflurane. Dexamethasone, atropine and ampicillin were administered preoperatively and ampicillin and ketoprofen were given post-operatively.

Cortical implant and recording

For recording electrocorticogram (ECoG), I chronically implanted a multichannel electrode array (Unique Medical Corporation, Tokyo, Japan) in the subdural space in two monkeys (monkey TE and M). ECoG electrode array is

containing 2.1mm diameter platinum electrodes (1mm diameter exposed from a silicone sheet) with an inter-electrode distances of 3mm. Thirty electrodes were implanted in the left hemisphere in monkey TE, and 45 electrodes were implanted in the left hemisphere, covering from the prefrontal cortex (PFC) to the primary somatosensory cortex as shown in Fig 4A. The reference and ground electrode were also placed in the subdural space. For recording of local field potential (LFP), monkey TA was chronically implanted with twenty hand-moveable tungsten microwire electrode array (Jackson and Fetz, 2007) in M1. Electrical cables leading from the electrode array were connected to connectors anchored to the skull with titanium screws. The cortical electrodes and the head-post chamber were anchored to the screws and acrylic cement. The electrode arrays were connected to a 128-channel amplifier (Cerebus; Blackrock Microsystems) with a gain of 1000, and signals from each electrode were sampled at 10 kHz.

Surgery for muscle stimulation

Bipolar stimulating wires were implanted surgically (Monkey M and TA) or transcutaneously (monkey TE). Electrical stimulus applied with electrodes with electrodes surgically implanted in arm, wrist, and hand muscles in total of fifteen muscles in monkey M and twelve muscles in monkey TA, identified by anatomical

features and by movements evoked by trains of low-intensity stimulation. Bipolar, multi-stranded stainless steel wires (AS633, Cooner Wire, Chatsworth, CA, USA) were sutured into each muscle and wires were routed subcutaneously to a connector on the animal's head. In monkey TA, electrodes were implanted in shoulder muscles (deltoid, del), elbow muscles (triceps ,tri; biceps brachii, BB), wrist flexor muscles (carpi radialis, FCR; palmaris longus, PL; pronator teres, PT; digitorum sublimis, FDS; carpi ulnaris, FCU), wrist extensor muscles (carpi ulnaris, ECU; digitorum communis, EDC; carpi radialis, ECR; brachioradialis, BR), and digit muscles (digitorum 4&5, ED45; abductor pollicis longus, APL; adductor pollicis, ADP). In monkey TA, electrodes were implanted in elbow muscles (Tri, BB), wrist flexor muscles (FCR, PL, FDS, FC), wrist extensor muscles (ECU, EDC, ECR, BR), and digit muscles (extensor digitorum 2&3, ED23; first dorsal interosseous, FDI). In monkey TE, I stimulated synergistic muscles transcutaneously, which was confirmed by the visual inspection and the stimulus-evoked movements before ACMC sessions. During ACMC session, two synergist muscles (e.g., wrist flexors or extensors) were selected for stimulation. The electrical stimulation was delivered through the stimulator (FHC, Bp Isolator, Bowdoin, USA).

Surgery for Stroke model

The stroke model was made by occluding the lenticulostriate arteries (LSA) in monkey TA and M. In monkey TE, I occluded both the LSA and the anterior chroidal artery (AChA) (**Fig. 1**). In order to expose the origin of LSA and AChA, which arises just proximal to top of the internal carotid artery (ICA), I used left frontotemporal approach. The animals were fixed to a stereotaxic frame in supine position with their head rotated 15° toward the right side. After the removal of bone flap, the dura was opened. Left frontal lobe was elevated to expose the optic chiasma and ICA. ICA was traced proximally to identify the origin of AChA which arises from posterior wall of ICA and courses along with optic tract. AChA was coagulated and transected at just distal to the origin of AChA. ICA was traced distally to identify the horizontal portion of middle cerebral artery (MCA). The arachnoid and trabecula around the MCA were dissected out to expose the origin of LSA which arises anterosuperiorly from MCA. LSA were coagulated and transected. Dura was sealed and cranioplasty with Polymethyl methacrylate (PMMA) was performed.

Artificial corticomuscular connection (Conversion of brain activity to electrical stimulation)

To achieve an artificial corticomuscular connection (ACMC) that sends voluntary commands to the paretic muscles and bypasses the stroke, cortical oscillatory activity was converted to stimulus pulses. An ACMC was accomplished by a computer interface which was designed to detect the particular neural oscillations by the template matching algorithm and converted in real-time to activity-contingent electrical stimuli dependent on that of the firing frequency.

Before ACMC session, I set a few minute period in which the monkey viewed a blank screen to discriminate the particular waveforms of filtered high-gamma oscillations (80-120 Hz) were identified by a spike-sorting device based on a template-matching algorithm (MSD, Alpha Omega Engineering). The particular high-gamma waveforms with relatively high amplitude which was used for the input signal of ACMC were selected to reliably discriminate from the stimulus artifacts. Thus, despite stimulus artifacts present in the recordings, stimulus artifacts were sufficiently brief to preserve >86 % of simultaneous neural signals for discrimination, and their shapes were reliable separable from the neural oscillations. To minimize artifacts, stimuli delivered to two synergistic muscles were simultaneous.

The moving averaged frequency (250 ms time window) of the selected high-gamma neural events has a proportional relationship with both stimulation current

and frequency, so that monkeys could voluntarily alter both the current and frequency of electrical stimuli. If the averaged frequency of selected high-gamma neural oscillation (X [Hz]) was above stimulus threshold (X_{th} [Hz]), stimulus frequency (f [Hz]) and current (I [mA]) were modulated by the equations as follows;

$$f = f_0 + \frac{f_g}{X_{th}} \cdot X, (f_0 \leq f \leq f_{Max}) \qquad \text{eq.1}$$

(f_0 = the initial stimulus frequency when X [Hz] was above X_{th} [Hz], f_g = the gain of stimulus frequency, f_{Max} = maximum stimulus frequency [Hz])

$$I = I_0 + \frac{I_g}{X_{th}} \cdot X, (I_0 \leq I \leq I_{Max}) \qquad \text{eq.2}$$

(I_0 = the initial stimulus current, I_g = gain of stimulus current, I_{Max} = maximum stimulus current [mA])

Across the monkeys, these parameters ranged as follows; (X_{th}: 6.5-10 Hz, f_0: 5-10 Hz, f_g: 0.3-0.5 Hz, f_{Max}: 20-35 Hz in all subjects, I_0: 1.5-2.2 mA, I_g: 0.05-0.08 mA, I_{Max}: 3.4-4.5 mA).

The initial stimulus current (I_0), the initial stimulus frequency (f_0), and maximum stimulus current (I_{Max}) were sometimes adjusted to offset muscle fatigue and maintain a consistent relation between wrist torque and selected high-gamma frequency. However, improvements in target success rates were not due to changing task difficulty or stimulus gain, as target parameters and gain were not significantly different. I

selected a pair of synergistic muscles as the stimulus muscles. After confirming the direction of evoked movements, the target was set on the direction which was corresponded to the direction of evoked movement or torque.

Behavioral task

Monkeys controlled the one-dimensional position of a cursor on a video monitor with isometric flexion and extension wrist torques (the torque-tracking task) or position (position-tracking task), and acquired targets displayed on the screen. The monkey was required to maintain torque within each target for 0.5–1.8 s to receive a juice reward. Targets remained on the screen until the hold criterion was met, followed by presentation of the next target, either immediately or after a variable reward period. Monkeys were performed in total 108 sessions with ACMC of the torque-matching task (monkey TE: 11 sessions, monkey TA: 28 sessions, monkey M: 33 sessions), or the position-tracking task (monkey TA: 32 sessions, monkey M: 4 sessions). Some sessions were set two-graded force matching task (monkey TA: 19 sessions, monkey M: 12 sessions), or two-graded position-tracking task (monkey TA: 17 sessions).

Results

Three adult male macaque monkeys (monkey TE, M, and TA) were trained to perform visually-guided center-out reaching movements with their wrist. Following implantation of electrocorticogram (ECoG) on the cortical surface over the sensorimotor areas (Monkey TE and M), or microelectrode array to the primary motor cortex (Monkey TA), I induced focal ischemia at the corona radiata level by embolization of the lenticulostriate and/or anterior coronary arteries. After stroke, the lesion was found to include the cerebral peduncle, corona radiata caudate and putamen, but the cerebral cortex appeared to be largely intact (**Fig. 1**). In addition, I confirmed all the monkeys completely showed near complete paralysis in their digits, wrist, and elbow after the stroke and did not recover during the present experimental period of 1 month.

The stroke monkeys were connected to the AMAC, by which high-gamma neural activities recorded from the single electrode in premotor cortex (PM), or primary motor cortex (M1), or primary somatosensory cortex (S1) was used to trigger stimulation of paretic muscles. In each session, the input signal was determined by filtering-in the high-gamma band (80-120 Hz) signal and arbitrary-discriminating a particular waveform by the template matching method. To allow the monkeys to grade the contraction force of their wrist muscles, current intensity and frequency of the

stimulation were determined linearly proportional to the smoothed frequency of the discriminated high-gamma waveform when its frequency exceeded the predetermined threshold level. Then, the monkeys demonstrated volitionally control of the paretic upper limb through ACMC (**Fig. 2A**).

Volitional control of paretic hand through ACMC in stroke monkey

Fig. 2B shows a typical example of task performance of the force-tracking task with the stroke monkey connected to the ACMC with input signal taken from an electrode in the M1 (monkey TA). During ACMC (green bar), the monkey was able to modulate stimulation volitionally, thereby could repeatedly acquire the target. To demonstrate that the ACMC was necessary, the stimulation was sometimes briefly turned off ("catch trials" (white bar)). Then, the monkey continued to make efforts to acquire the targets, as evidenced by significant increase in the averaged frequency of the selected high-gamma waveforms, but the wrist was completely paralyzed and the monkey did not succeed in acquiring the targets at all. In some sessions, the monkeys were tested in three-grade position-tracking task (**Fig. 3**). The monkey could successfully acquire each target by controlling the stimulation. I applied the ACMC in three stroke monkeys in a total of 108 sessions (duration of sessions: 6-74 min; range of

trial numbers within each session: 55-965 trials), using 92 different pairs of cortical sites and muscles (**Fig. 4)**. Task performance was rapidly improved within 20 minutes ($p<0.05$, **Figs. 4B** and **C** in population data; and see results of each monkey in **Fig. 5A**) after start of using a particular electrode signal for the input, suggesting that the monkeys could learn to utilize the ACMC by themselves. The averaged task performance in the ACMC trials across monkeys and input electrodes was substantially higher than those in catch trials, indicating that the ACMC was necessary to get the target ($P<10^{-23}$; left panel in **Fig. 4C**).

In each session, I randomly changed the input electrode for controlling ACMC, among those located over PM, M1, and S1 (**Fig. 4A**). Thus, I next compared the task performance with the input signals from electrodes located in PM, M1, and S1. The task performance significantly improved in late phase compared with initial phase with the input electrode either in PM ($P<0.05$), M1 ($P<0.01$), or S1 ($P<0.05$). Second, there was not any significant difference of task performance with the input electrode in either of these cortical areas ($P>0.05$), indicating that the monkeys could control neural activity of any of the regions over PM, M1, and S1 to be adapted to the ACMC (**Fig. 4C** in population data, and see results of each monkey in **Fig. 5B**).

Volitional modulation of input signals from various cortical regions

To understand the neural mechanism underlying adaptation to the ACMC, I analyzed the task-related modulation depth of input signals during initial and late phases in each session. Modulation depth was defined as the ratio of the input signal (i.e. the averaged frequency of the selected high-gamma waveform) for one second before and after the target appearance. Along with increase in task performance (**Fig. 6A**), I found significant increase of modulation depth of the input signal during late phase compared with initial phase (**Fig. 6B**). This result suggested that the monkey learned to effectively produce the stimulation as the output signal to paretic hand in response to the target appearance, and finally became able to reach rapidly and successfully to the target through learning. The population analysis of modulation depth of the input signal also indicated the significant increase during late phase compared with the initial phase ($P<0.05$). Moreover, the increase of task-related modulation by learning was observed for the various input electrodes located over PM ($P<0.05$), M1 ($P<0.01$), and S1 ($P<0.05$) (**Fig. 6C**). However, there was any significant difference in modulation depth among cortical areas ($P>0.05$), suggesting that the monkeys could be flexibly adapted to the newly-given various input electrodes for controlling ACMC by increasing the signals from the arbitrarily assigned input electrodes.

Large-scaled reorganization during learning

To further investigate the neural mechanism underlying the learning-related modulation of the input signal, I next investigated the modulation depth of high-gamma power (80-120 Hz) across all the recorded ECoG electrodes, which include with the input electrode and all the other non-input electrodes those distributed extensive cortical area. Since I selected the high-gamma waveform with relatively high amplitude as the input signal (see **Methods** in details), the modulation depth of the high-gamma power was calculated for quantifying the input-related neural signals in each electrode. **Fig. 7A** and **B** shows a typical example of improvcement of the task performance with the input electrode over M1, and the changes in the modulation depth of high-gamma power in each learning phase (i.e. initial, early, mid, and late phases for 25 min learning period) over the wide cortical area recorded through 45 ECoG electrodes (see also **Fig. 8** in results of other monkey). I could observe the gradual change in the topographical organization of the modulation depth over the large-scaled cortical areas as a function of the time course of learning. In the initial phase, the modulation depth was distributed with relatively uniformity over the recorded areas. In the early and middle phases, however, the modulation depth increased around prefrontal cortex (PF), PM, and lateral

portion of S1. In the late phase, the “hot spots” of modulation depth expanded over S1 and included the input electrode in M1, while the hot spot around PF and PM gradually shrank over time. Eventually, the “hot spot” of modulation depth was concentrated around the selected input electrode in M1. This tendency was more obvious if the data were analyzed on the difference of modulation depth (**Fig. 7C**). The difference of modulation depth between the initial and early phases indicated the increase of the activation area in PF, PM, and lateral portion of S1, which were located relatively distant from the input electrode. On the other hand, the difference of modulation depth between initial and late phases indicated that the increase in modulation depth in PF, PM, and S1 areas diminished, whereas the modulation depth close to the input electrode in M1 increased over time, indicating that the monkey finally learned to focus the area of activation around the arbitrarily-selected input electrode. This result was consistent also in the sessions in which the input electrode was located in S1 (**Fig. 9**) and PM (**Fig. 10B** and **C** in session 3).

Rapid and flexible large-scale cortical adaptation to ACMC

Finally, to clarify the flexibility of adaptation to ACMC and the underlying neural mechanism, I investigated the difference of the modulation depth map when the

input electrode was suddenly shifted among different areas within a day. **Fig. 10** shows a typical example of the task performance and the difference of the modulation depth map in three successive sessions. On this day, the input electrodes were assigned in medial portion of M1 for session 1, lateral portion of M1 for session 2, and rostromedial portion of PM for session 3, which were widely-separated from each other. However, the monkey could rapidly increase the task performance in each session (**Fig. 10A**), suggesting that the monkey could flexibly re-learn ACMC with the newly assigned input electrodes. Along with the increase of the task performance, the monkey has changed the modulation depth of the high-gamma power in each session (**Fig. 10B**). Interestingly, the difference of modulation depth suggested that the area of the strongest modulation was concentrated close to the input electrode in each session (**Fig. 10C**), indicating that the monkey could regulate the high-gamma modulation depth to the newly given input electrode across the large-scaled cortical sensorimotor area.

In another series of sessions within a day, I changed the input electrode to the neighboring electrode within PM (**Fig. 11**). The learning effect has been carried over the preceding session, in which the performance in the initial phase of next session was comparable to that in the late phase of the preceding session (**Fig. 11A**). With the remaining learning effect, the monkey could also maintain the modulation depth of

high-gamma power in the next session as evidenced by the result of non-significant change in modulation depth in the next session compared with the preceding session (**Fig. 11B** and **C**). This result suggested that the monkey could effectively use the remaining learning effect depending on the relative location of the input electrodes among the sessions.

Finally, I analyzed the averaged changes in the modulation of high-gamma power between initial and late phases among sessions, suggesting that the areas with the strongest high-gamma power modulation was located around the input electrodes, although modulation depth of the high-gamma power was globally increased among the large cortical areas (**Fig. 12**). This result suggested that to utilize the ACMC, the monkeys could learn to increase the high-gamma power modulation focally close to the input electrode which was randomly-assigned from cortical areas in PM, M1, and S1.

Discussion

This study was the first demonstration that the monkeys with extensive subcortical damage after stroke could restore the impaired volitional control of one-dimensional movement in the paretic hand through ACMC. Surprisingly, although the damaged area included basal ganglia, whichplays an important role of reinforcement learning (Ito et al., 1982; Doya. 2000; Izawa et al., 2001) the monkeys still had an adequate adaptability to control ACMC. The adaptation was rapid, flexible and induced by learning to modulate the arbitrarily-selected high-gamma input signal which was recorded from randomly-assigned single electrode placed either in PM, M1, or S1. Notably, during adaptation to ACMC, a large-scaled reorganization of input-related high-gamma activity was observed, in which cortical areas with the strongest high-gamma modulation was focused on the area close to the input electrode. Moreover, when the input electrode was moved over long distance across the areal border from the previous input electrode, the monkeys could still re-learn the newly assigned ACMC arrangement by rapidly changing the high-gamma modulation around the updated input electrode. These findings indicated that monkeys with extensive subcortical damage after stroke had an adequate adaptability to control the closed-loop neuroprosthesis.

One of the main findings in this study was the flexibility of the damaged-brain

in controlling the neural signal used for neuroprosthetic device. A goal of the field of BMI research is to enable skilled control of paretic extremities or external actuator via BMI while minimizing the learning required (Taylor et al., 2002; Ganguly et al., 2009; Nicolelis et al., 2009). In other words, it must be an essential problem whether neuroprosthetic control can be achieved in a rapid and flexible manner. In support of this goal, previous BMI studies have demonstrated that quadriplegic patients could volitionally modulate the activity of neurons in the motor cortex after years of paralysis (Hochberg et al., 2006; Hochberg et al., 2012), and that monkeys could use cortical activity to control a robotic arm to acquire targets (Carmena et al., 2003; Ganguly et al., 2009; Ganguly et al., 2011), grasp (Either et al., 2012) and feed themselves (Velliste et al., 2008). In these researches, however, the controlling signal was evaluated with sophisticated algorithms of biomimetic decoders that capture the original relationship between neural activity and a movement parameter. An alternative strategy to restore the impaired function is to directly connect cortical activity to control the stimulation of a patient's paralysed muscles (Moritz et al., 2008). However, it still remained unclear whether subjects with damaged-brain have also an essential capacity to control such a closed-loop neural prosthesis. I found that the monkeys with extensive subcortical damage after stroke could rapidly get adapted to ACMC by modulating the firing rates

of arbitrarily selected high-gamma waveforms (**Fig. 6B**). Interestingly, in my paradigm I used an arbitrarily-selected high-gamma waveform as the input signal for controlling ACMC (see **Methods** in detail), which was unsure to have an association with actual wrist movement. This was partially because there was no opportunity to record movement-related neural signal due to severe paralysis of monkeys after stroke. Nevertheless, the monkeys equally learned to control the arbitrarily-assigned input signal recorded from a large cortical areas including PM, M1, and S1 (**Fig. 4C**). Previous studies of operant conditioning of neural activity using biofeedback have shown that cells in PM (Nishimura et al., 2013a), M1 (Fetz and Baker, 1973; Fetz and Finocchio, 1975; Moritz et al., 2008; Nishimura et al., 2013a), or S1 (Moritz and Fetz, 2011) with no discernable relation to muscles can be volitionally modulated after brief practice sessions. However, important difference between previous studies and my current study was that my paradigm did not set operant conditioning task before ACMC session, which might have given the opportunity to learn to associate the input signal with a computer cursor. This suggested that the monkeys with stroke still had a capacity to learn the causal link between arbitrarily-selected input signal and output wrist movements thorough muscle stimulation without associating the input signal with a cursor in pre-operant conditioning task. Therefore, these results could expand the

possible range of picking up the controlling signals for BMIs with wide clinical application.

Another advantage of my protocol might be to use the thin and flexible structure of the ECoG array, which allowed us to detect the cortical signal with higher-accuracy and less invasiveness (Rubehn et al., 2009; Watanabe et al., 2010; Shin et al., 2010). ECoG electrodes do not penetrate the cortical surface, thereby reduces the potential risk for brain tissue damage and increasing long-term stability for recordings (Chao et al., 2010; Chen et al. 2013; unpublished observation of my study). In case of recording with ECoG, the power of high-gamma oscillations was clearly modulated before or around the onset of movements (Crone et al., 1998; Anderson et al., 2012). Thus, recent studies have shown that ECoG signals in high-gamma frequency range carry rich information sufficient for decoding a set of arm movements (Leuthardt et al., 2004; Mehring et al., 2004; Yanagisawa et al., 2012), and were suitable controlling signal for ECoG-based BCI (Miller et al., 2007, 2008; Yanagisawa et al., 2012; Wander et al., 2013). Notably, I further demonstrated that the ECoG-based closed-loop neural prosthesis could be established in subjects with stroke for restoration of impaired limb functions. However, it is to be noted that residual stimulus artefacts made discrimination of input neural signal difficult and less accurate. In my paradigm, I used a

template-matching method to discriminate in-real time the particular high-gamma waveform from the residual stimulus artefacts. As a result, formation of a positive reverberating loop could be avoided during ACMC session (unanalyzed results), and I could establish highly accurate neuroprosthetic control. Overall, these results suggested that my protocol is well suited for clinical application for restoration of impaired limb function in individuals with stroke.

Notably, I found that reorganization of the input signal occurred very rapidly within 20 min, and the sites for strongest high-gamma modulation has been finally focused on the randomly-assigned input electrode (**Fig. 7C**). This shifting of activation to the input electrode could be observed among various input electrode sites including PM (**Fig. 9**), M1 (**Fig. 9** and **8**), and S1 (**Fig. 10**). Such ability of the brain to adapt to new but consistent sensorimotor contingencies has been documented in the previous studies. Motor cortex can adapt rapidly to learn new motor skills (Shadmehr et al., 1994; Thach et al., 1978). Motor circuitry can compensate for drastic changes in connectivity, such as surgically cross-connected nerves controlling wrist flexor and extensor muscles (Gandolfo et al., 2000; Nudo et al., 1996), or targeted reinnervation for control of prosthetic limbs (Brainkman et al., 1983; Kuiken et al., 2004; Kuiken et al., 2007). However, in these previous studies, cortical reorganization was induced in

much longer time scale (i.e. several hours or days), thereby different underlying mechanisms may contribute to the rapid cortical reorganization shown in my present study. Similar rapid changing in BCI-related neural modulation have been recently reported in a human ECoG-based BCI study (Wander et al., 2013), which reported that when learning a BCI task using high-gamma activity recorded from motor cortex, a learning-related network reorganization was observed in a large-scaled cortical areas. In this study, as the subjects became proficient, strong initial task-related activation around input electrode was followed by decreasing of activation in PF, PM, and posterior parietal cortex, areas that have previously been implicated in the cognitive phase of motor sequence learning and abstract task learning (Schlaug et al., 1994; Jenkins et al., 1994; Hikosaka et al., 2002). This change of high-gamma modulation may reflect mental shift from cognitive to automatic task execution during the BCI task, which can be related to my present study. Indeed, during learning of ACMC, monkeys could use the somatosensory feedback via artificial stimulation to the muscles as well as the visual feedback via the movement-related information on the screen, although the sensory evoked potential was substantially reduced among recorded cortical sites after stoke (data not shown). In this aspect, the initial increasing modulation surrounding PF and S1 might reflect the initial cognitive phase, while the late phase in which the

modulation depth increased near the input electrode may represent the automatic control phase. However, my novel point is even if the input electrode was applied to different areas among PM, M1 S1, the strong task-related modulation could be flexibly focused on the selected input electrode Therefore, future experiments are needed to resolve the underlying mechanism of these rapid flexible reorganizations.

These consequences of previous and my studies lead to a fundamental question that which regions in the brain are responsible for the learning to closed-loop neuroprosthetic control. Recent work performed by Koralek and colleagues (2012) has demonstrated that the striatum is involved in and critical to development of proficiency with a BCI in a rat model. This finding was notable, given that effective use of the BCI did not explicitly require recruitment of the motor system outside of motor cortex, yet task performance was degraded in subjects with impaired cortico-striatal interaction. However, in the present study, to my surprise, even if monkeys had extensive subcortical damage including the putamen, they could still get adapted to ACMC very rapidly and flexibly. Such differences might be explained by the difference in the type of neruoprsthetic learning, that is, the previous study required more emphasis on the abstract learning without physical movements, while my paradigm required more physical learning under the control by the input signal, which was a more complex

situation. Other studies have demonstrated the vital and differential roles between the basal ganglia and cerebellum during motor sequence learning and motor adaptation (Dayan and Benalis, 2005; Hikosaka et al., 2002). However, the involvement of these subcortical networks in the process of BMI skill acquisition remains an open question, from both the basic neuroscience point of view and the incremental improvement of BMI frameworks. In either case, a logical and necessary extension of these findings is to investigate the roles that the subcortical networks play in the same learning process.

Figure Legends

Figure 1. Stroke model in monkey

A: Transaxial T2-weighted MRI images shows the lesion extent in monkey TE. Red lines represent the lesion area which included in the temporal lobe (TL in a), cerebral peduncle (CP in a), putamen (Put in b), caudate (Cau) and corona radiate (CR in c).

B: Lines drawn on the coronal view of the brain in C correspond to the levels of transaxial sections of (a–d) in A

C: The table shows the artery of embolization in each monkey.

Figure 2. Volitional control of paretic hand through an artificial corticomuscular connection (ACMC)

A: Schematic shows an ACMC, cortical oscillatory activity converted to electrical stimulation in paretic muscles. The raw signal recorded from single selected ECoG electrode over cortical areas was delivered to decoder, in which raw signal was filtered in the high-gamma frequency band (80-120 Hz), and the particular high-gamma oscillations were discriminated to dissociate from the artifact of the electrical stimulation. The instantaneous frequency of selected particular high-gamma oscillations

was smoothed, then the wave form for stimulation was produced and applied to the paretic hand muscles. Stimulus current and frequency were made linearly proportional to the smoothed frequency of discriminated high-gamma oscillations when this was above the threshold.

B: Representative example of five successful trials with the artificial corticomuscular connection (ACMC, green) and one catch trial (gray shading) in monkey TA. Stimulation was delivered to muscles with frequency (6^{th} low) and current (7^{th} low) proportional to high-gamma events above a stimulation threshold (The blue horizontal line in 5^{th} low). During the catch trial, although the monkey made attempts to produce wrist torque as seen in the increasing frequency of selected high-gamma events, the monkey failed to acquire the target because of the paralysis. Blue vertical lines in 1^{st} and 2^{nd} lows indicate the timing of the electrical stimulation. Red traces in 3^{rd} low indicate the discriminated gamma events which were used to control stimulus. The blue rectangles in trace of wrist torque target. From top, raw signal recorded from the input electrode, high-gamma signal (80-120Hz), discriminated high-gamma waveforms (red lines), stimulus frequency, stimulus current, and wrist torque. Arrows indicate times of successful task completion and reward.

Figure 3. Volitional control of paretic hand during three-graded position-tracking task with ACMC

Representative example of six successful trials with ACMC (green) and a catch trial (gray shading) during three-graded position-tracking task in monkey TA. Figure arrangement corresponds with figure 2.

Figure 4. Task performance with the ACMC

A: Electrode locations in three monkeys. In monkey TE and M, ECoG electrodes were placed on the surface of the premotor cortex (PM, yellow circle), primary motor cortex (M1, red circle), and primary somatosensory cortex (S1, blue circle). The electrodes which were used for ACMC sessions as the input signal were circled in black solid lines. In monkey TA, twenty microelectrodes were implanted in the M1 hand (red dots). All electrodes were used for ACMC sessions.

B: Averaged task performance with the ACMC over twenty minutes across the session in three monkeys, showing task performance gradually increased over time. Error bars represent standard deviation.

C: Average task performance with the ACMC during five minutes of initial and late phases and during catch trials across sessions in three monkeys represented in the left.

Error bars represent standard deviation. Averaged task performance during five minutes of initial and late phases with the ACMC in which the input signal was located in PM (yellow), M1 (red), and S1 (blue) represented in the right.

Figure 5. Task performance in each monkey

A: Time course of task performance with the ACMC in three monkeys (left, monkey TE; middle, monkey TA; right, monkey M). Error bars represent standard deviation.

B: Task performance in different cortical areas in three monkeys (top, monkey TE; middle, monkey TA; bottom, monkey M). Error bars represent standard deviation. The input signals were recorded from various electrodes located in PM (yellow), M1 (red), and S1 (blue), but differ depending on monkeys.

Figure 6. Change in modulation depth of input signal during adaption to ACMC.

A: Electrode location showing on upper pannel. Time course of task performance using input electrode in M1 (Monkey TA) showing lower pannel.

B: Ensemble average of initial and late 20 trials in a representative session, aligned to the time of target appearance which was shown in black dotted line. From top, raster plot and averaged frequency of high-gamma events, stimulus frequency, and hand

position were shown. Blue shading rectangles in bottom trace represent the wrist position targets. The modulation depth was defined as the ratio of input signal before target appearance to that after target appearance, shown in blue dotted line (i.e. a/b=1.3 in initial phase, a'/b'=2.1 in late phase). Orange arrows represent the time of successful task completion and reward.

C: The averaged modulation depths of input signal in PM (yellow), M1 (red), and S1 (blue) during 20 trials of initial and late phases were shown. Error bars indicate the standard deviation.

Figure 7. Large-scale cortical reorganization in monkey M

A: The input electrode for ACMC showing red filled circle (a) Time course of task performance with ACMC using the input electrode over the M1 in monkey M. Modulation depth of high-gamma power was calculated the data obtained from the gray shading durations in initial, early, mid, late phases.

B: Topographic map of modulation depth of high-gamma power in initial, early, mid and late phases. Gray circle represents the input electrode. Black dots represent electrode location. The Value of the modulation depth was shown above the input electrodes in each panel, showing the values were gradually increasing over time.

C: Change in spatial distribution of modulation depth comparing initial to early, mid, and late phases were shown from left to right.

Figure 8 . Large-scale cortical reorganization in monkey TE

A: Time course of task performance during 20 min (b) with ACMC controlled by the input signal recorded from the electrode in M1 for monkey TE (a). Modulation depth of high-gamma power was calculated in the gray shading areas in initial and late phases.

B: Topographic map of modulation depth of high-gamma power in initialand late phases. Gray circle represents the input electrode, which was located in M1. C: Change in spatial distribution of modulation depth of high-gamma power.

Figure 9. Adaptation to ACMC with somatosensory cortex

A: Time course of task performance during 20 min (b) with ACMC controlled by the input signal recorded from the electrode in S1 for monkey M (a). Modulation depth of high-gamma power was calculated based on the gray shading durations in initial and late phases.

B: Topographic map of modulation depth of high-gamma power in initial and late phases. Gray circle represents the input electrode. Black dots represent other electrodes.

C: change in spatial distribution of modulation depth of high-gamma power in initial phase comparing to late phases.

Figure 10. Rapid large-scale cortical reorganization

A: Time course of task performance in three subsequent sessions with ACMC using widely separated input electrodes in each session over M1 and PM in monkey M. The input electrodes were shown in green circles, which were corresponded to shoulder area in M1 for session 1, digit area in M1 for session2, and shoulder area in PM for session 3. To evaluate the neuronal mechanism of adaptation process to ACMC with each input signal, the modulation depth of high-gamma power was calculated the data obtained from the gray shading durations in initial and late phases in each session.

B: Topographic map of modulation depth of high-gamma power in initial and late phases for three sessions. Gray circle represents the input electrode.

C: Change in spatial distribution of modulation depth of high-gamma power comparing initial to late phases in each session.

Figure 11. Carry-over effect of cortical reorganization

A: Time course of task performance in two continuous sessions using neighboring input electrodes showing by green circle as inset in each plot. Data obtained from monkey M

B: Topographic map of modulation depth of high-gamma power in initial and late phases for two sessions. Gray circle represents the input electrode.

C: Change in spatial distribution of modulation depth comparing initial to late phases in each session.

Figure 12. Change of modulation depth as a function of distance from the control electrode.

The averaged changes in the modulation of high-gamma power between initial and late phases among 6 sessions were analyzed in black line (left). Distance zero indicates the input electrode (vertical gray dotted line). The averaged changes of modulation with the input electrode in PM (yellow) and M1 (red) were shown in right side of the figure, suggesting that the areas in strongest high-gamma power modulation was located in the input electrodes, although the high-gamma power modulation globally increased among the large cortical areas.

Fig. 1

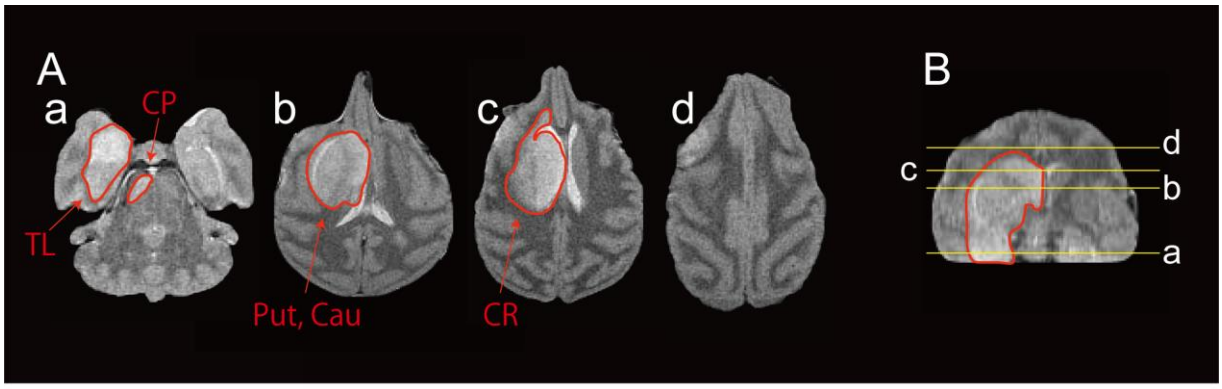

C

	Monkey TE	Monkey TA	Monkey M
Lenticulostriate artery	Occluded	Occluded	Occluded
Anterior choroidal artery	Occluded	Not occluded	Not occluded

Fig. 2

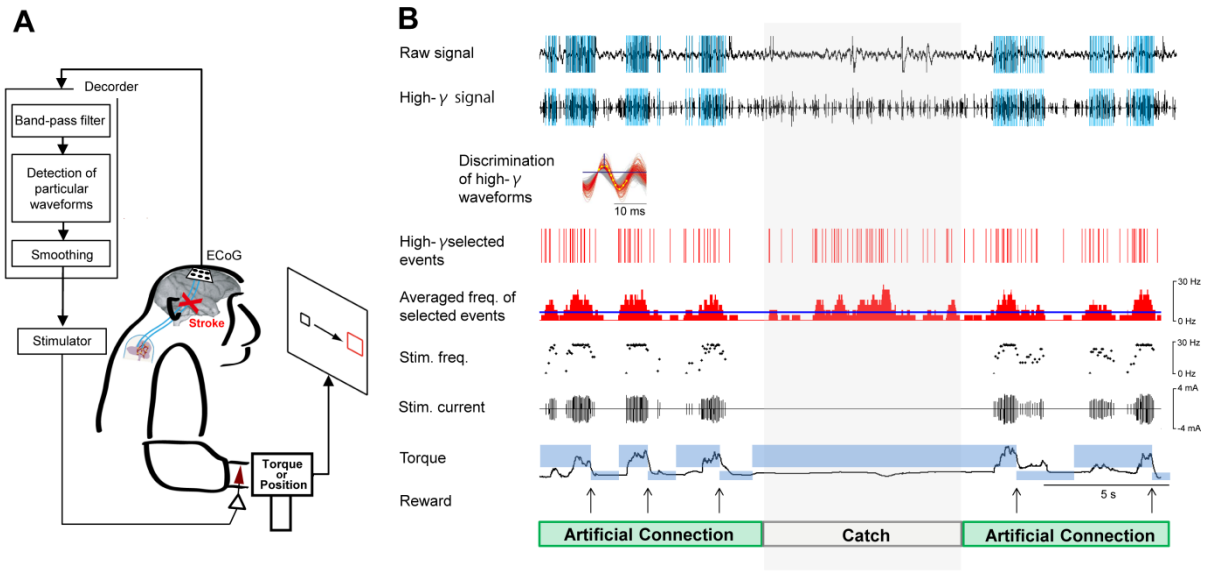
A
Decorder
Band-pass filter
Detection of particular waveforms
Smoothing
Stimulator
ECoG
Stroke
Torque or Position
B
Raw signal
High-γ signal
Discrimination of high-γ waveforms
10 ms
High-γselected events
Averaged freq. of selected events
30 Hz
0 Hz
Stim. freq.
30 Hz
0 Hz
Stim. current
4 mA
-4 mA
Torque
Reward
5 s
Artificial Connection
Catch
Artificial Connection

Fig. 3

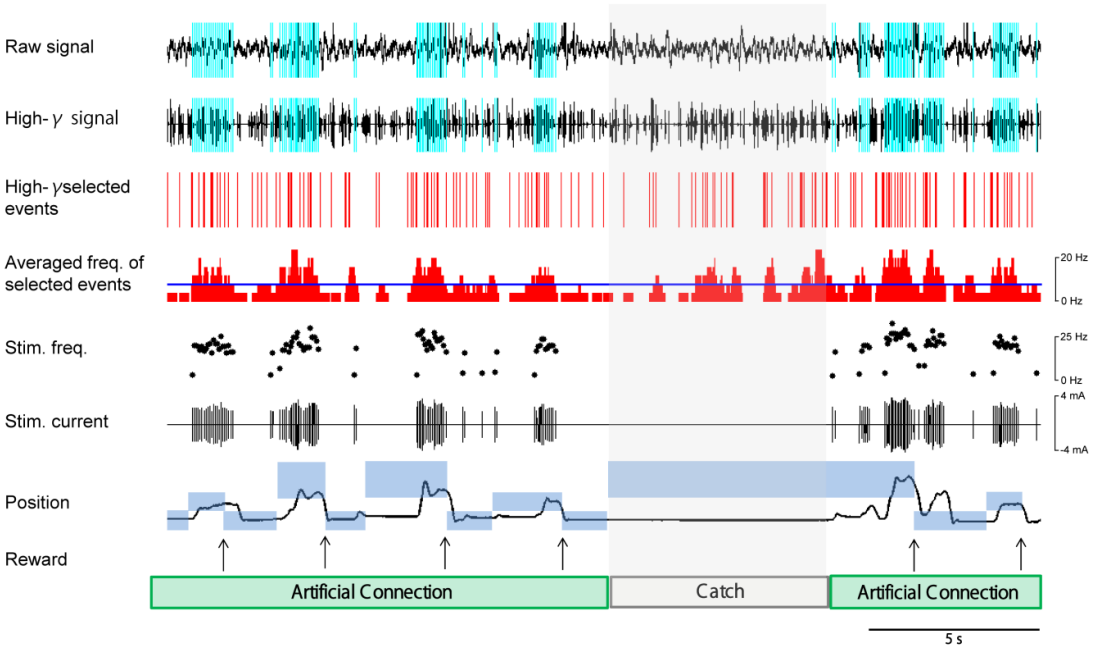
Raw signal
High-γ signal
High-γselected events
Averaged freq. of selected events
20 Hz
0 Hz
Stim. freq.
25 Hz
0 Hz
Stim. current
4 mA
-4 mA
Position
Reward
Artificial Connection
Catch
Artificial Connection
5 s

Fig. 4

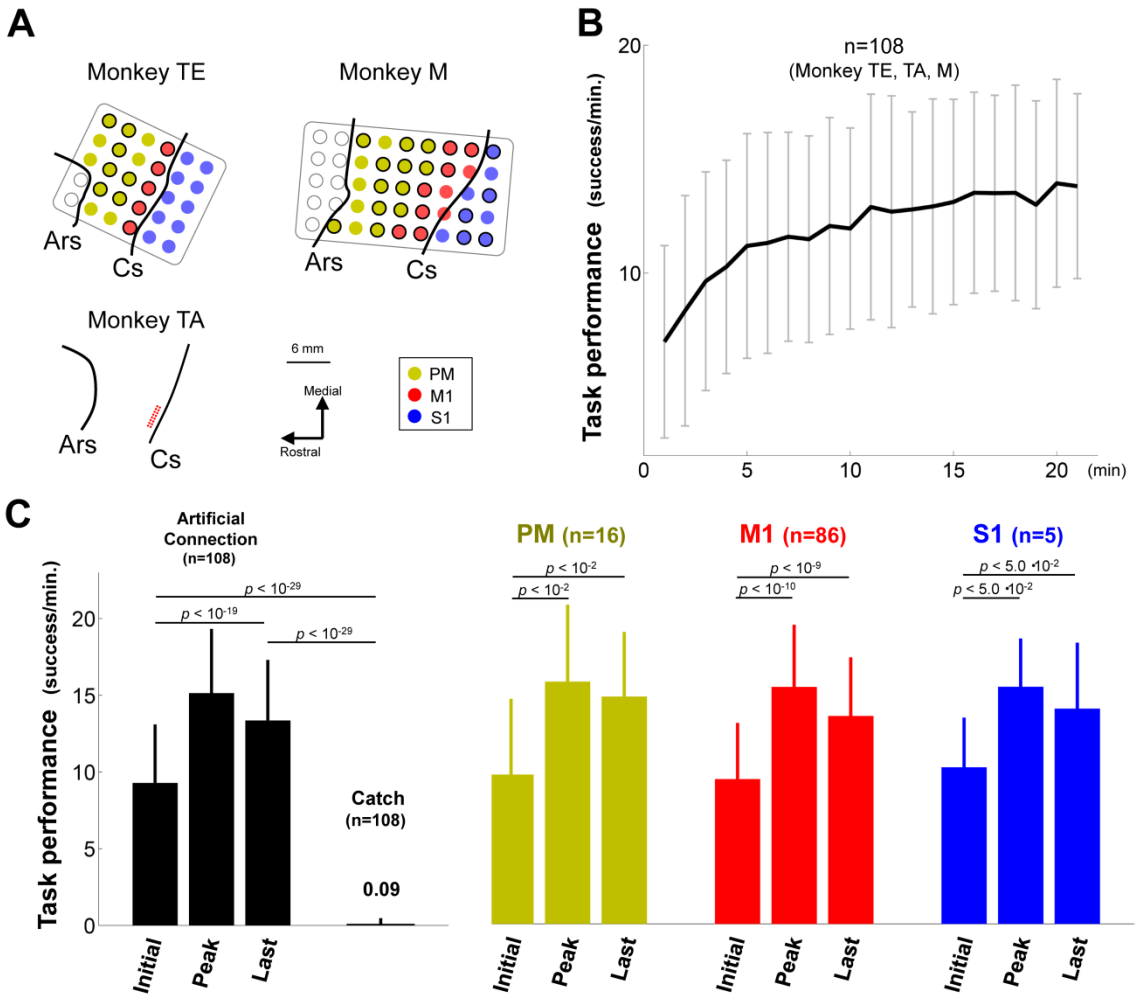
A
Monkey TE
Monkey M
Ars
Cs
Ars
Cs
Monkey TA
Ars
Cs
6 mm
Medial
Rostral
PM
M1
S1
B
n=108
(Monkey TE, TA, M)
Task performance (success/min.)
20
10
0
5
10
15
20
(min)
C
Artificial Connection (n=108)
p < 10-29
p < 10-19
p < 10-29
Catch (n=108)
0.09
PM (n=16)
p < 10-2
p < 10-2
M1 (n=86)
p < 10-9
p < 10-10
S1 (n=5)
p < 5.0 ·10-2
p < 5.0 ·10-2
Task performance (success/min.)
20
15
10
5
0
Initial
Peak
Last
Initial
Peak
Last
Initial
Peak
Last
Initial
Peak
Last

Fig. 5

A

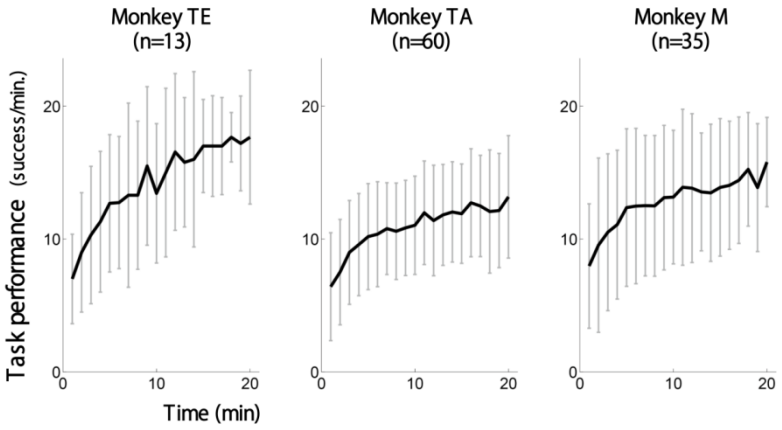
Monkey TE
(n=13)
Monkey TA
(n=60)
Monkey M
(n=35)
Task performance (success/min.)
Time (min)
0
10
20

B

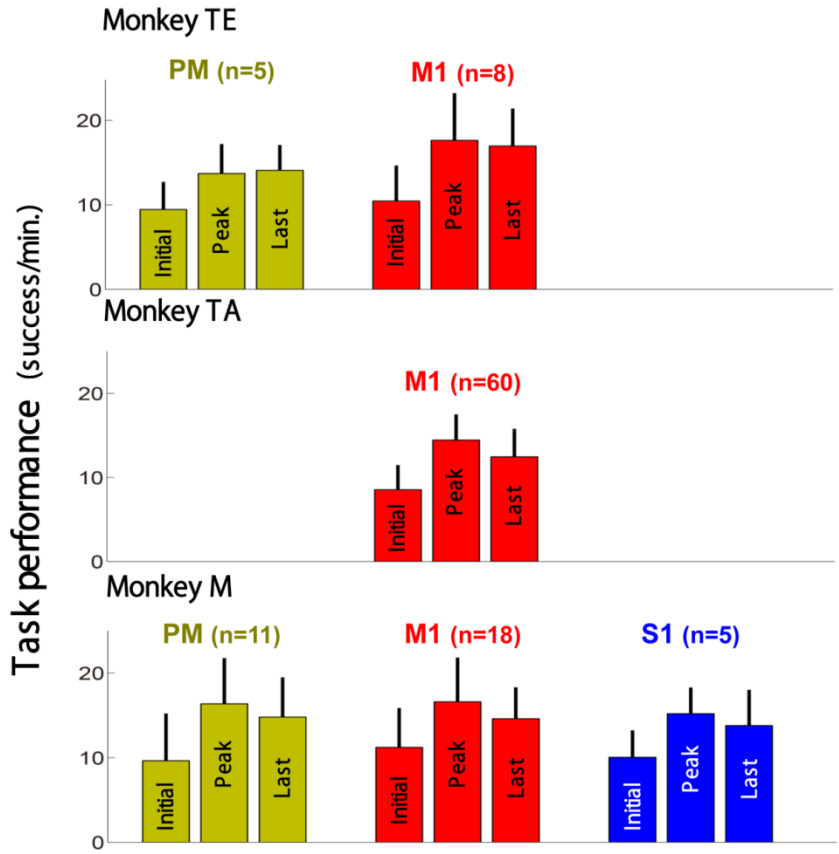
Monkey TE
PM (n=5)
M1 (n=8)
Monkey TA
M1 (n=60)
Monkey M
PM (n=11)
M1 (n=18)
S1 (n=5)
Initial
Peak
Last
Task performance (success/min.)
0
10
20

Fig. 6

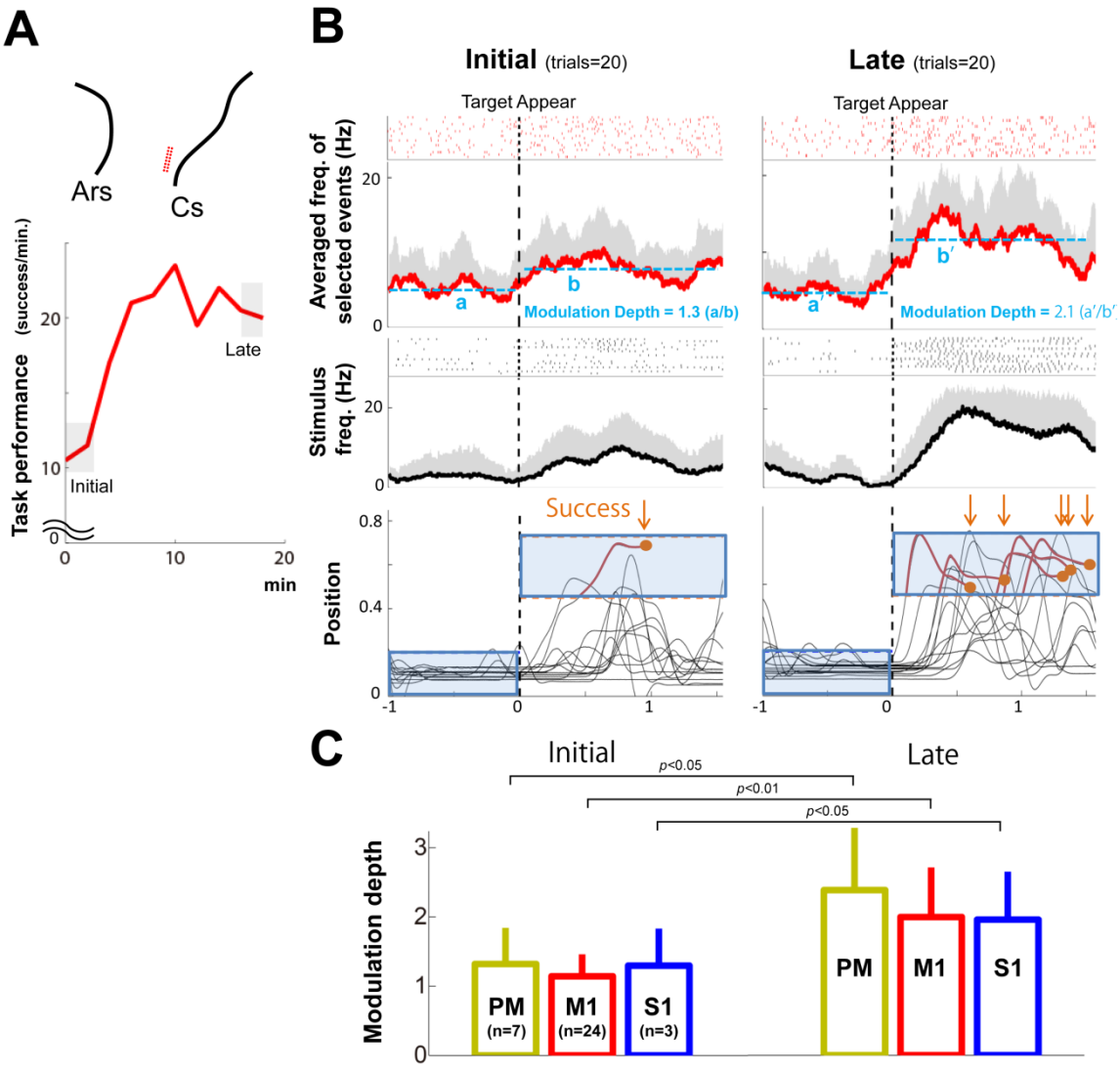
A
Ars
Cs
Task performance (success/min.)
20
10
0
Initial
Late
0
10
20
min
B
Initial (trials=20)
Late (trials=20)
Target Appear
Target Appear
Averaged freq. of selected events (Hz)
20
0
a
b
Modulation Depth = 1.3 (a/b)
a′
b′
Modulation Depth = 2.1 (a′/b′)
Stimulus freq. (Hz)
20
0
Success
Position
0.8
0.4
0
-1
0
1
-1
0
1
C
Initial
Late
p<0.05
p<0.01
p<0.05
Modulation depth
3
2
1
0
PM (n=7)
M1 (n=24)
S1 (n=3)
PM
M1
S1

Fig. 7

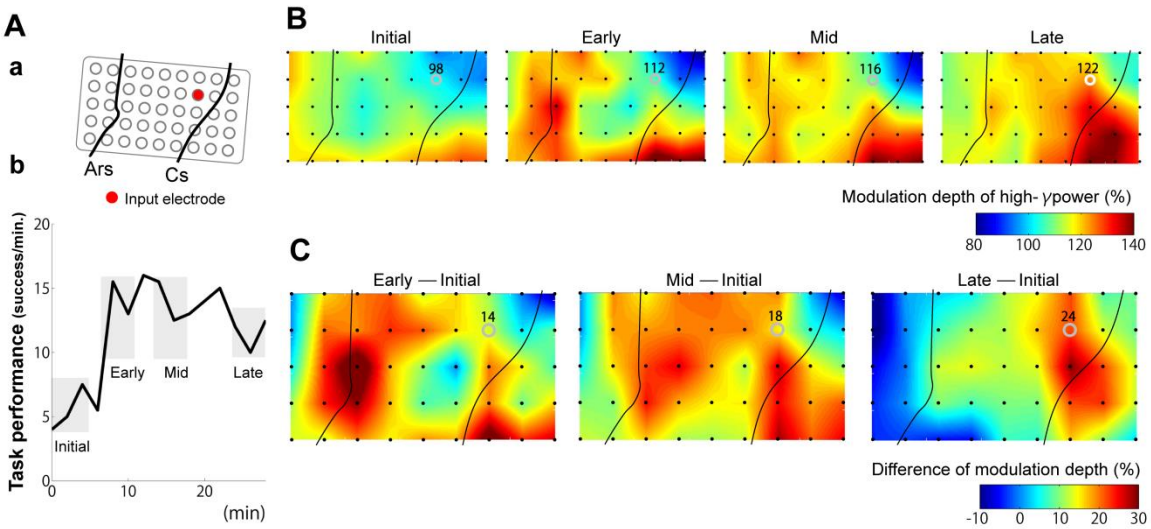
A
a
b
Ars
Cs
Input electrode
Task performance (success/min.)
20
15
10
5
0
0
10
20
(min)
Initial
Early
Mid
Late
B
Initial
Early
Mid
Late
98
112
116
122
Modulation depth of high-γpower (%)
80
100
120
140
C
Early — Initial
Mid — Initial
Late — Initial
14
18
24
Difference of modulation depth (%)
-10
0
10
20
30

Fig. 8

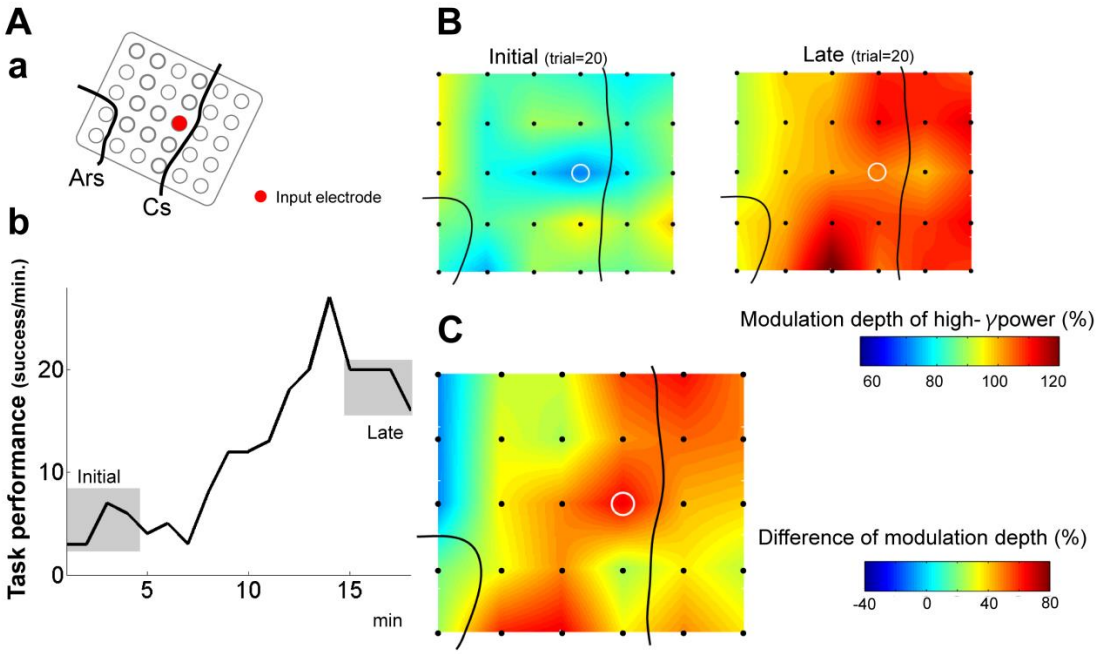
A
a
Ars
Cs
Input electrode
b
Task performance (success/min.)
20
10
0
Initial
Late
5
10
15
min
B
Initial (trial=20)
Late (trial=20)
C
Modulation depth of high-γpower (%)
60
80
100
120
Difference of modulation depth (%)
-40
0
40
80

Fig. 9

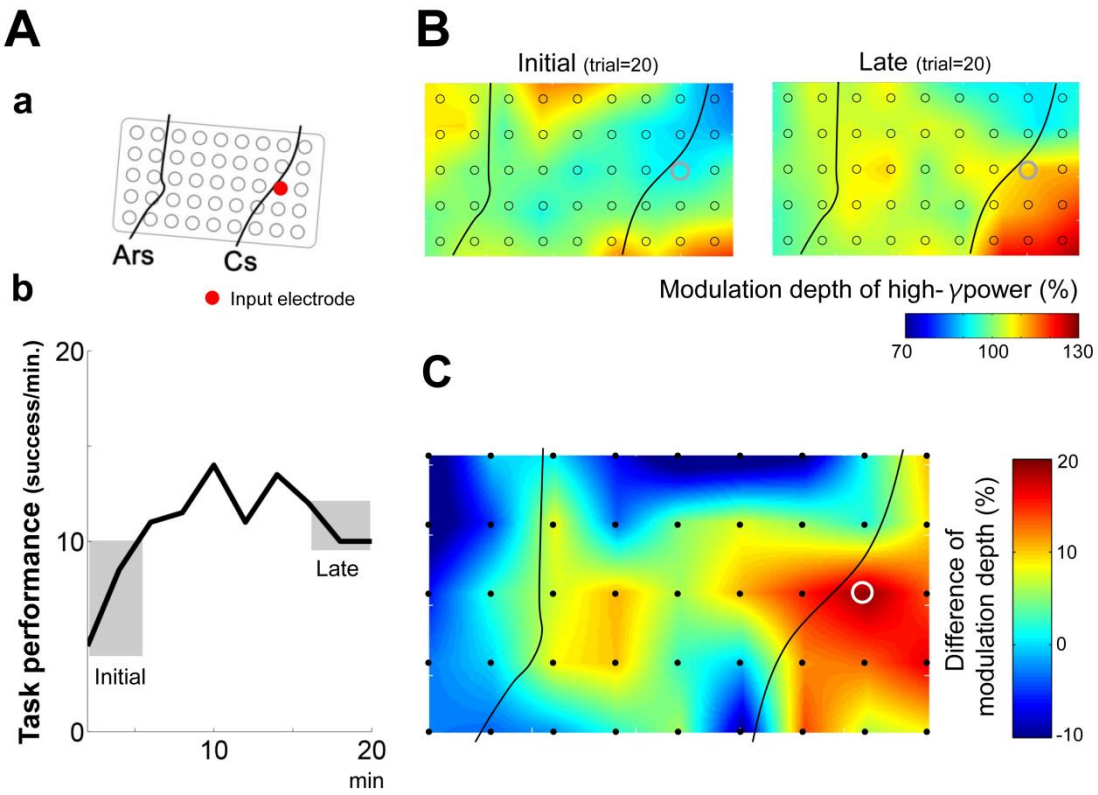
A
a
Ars
Cs
Input electrode
b
Task performance (success/min.)
20
10
0
10
20
min
Initial
Late
B
Initial (trial=20)
Late (trial=20)
Modulation depth of high-γpower (%)
70
100
130
C
Difference of modulation depth (%)
20
10
0
-10

Fig. 10

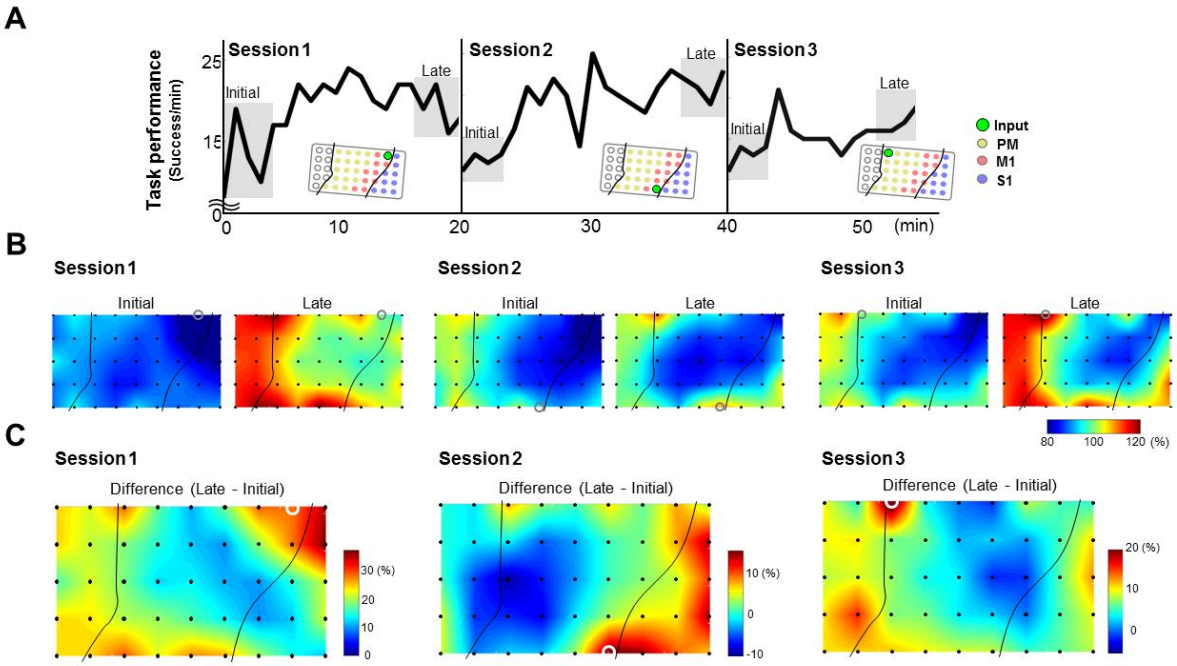
A
Session 1
Session 2
Session 3
Initial
Late
Task performance
(Success/min)
25
15
0
0
10
20
30
40
50
(min)
Input
PM
M1
S1
B
Session 1
Session 2
Session 3
Initial
Late
80
100
120 (%)
C
Session 1
Session 2
Session 3
Difference (Late - Initial)
30 (%)
20
10
0
10 (%)
0
-10
20 (%)
10
0

Fig. 11

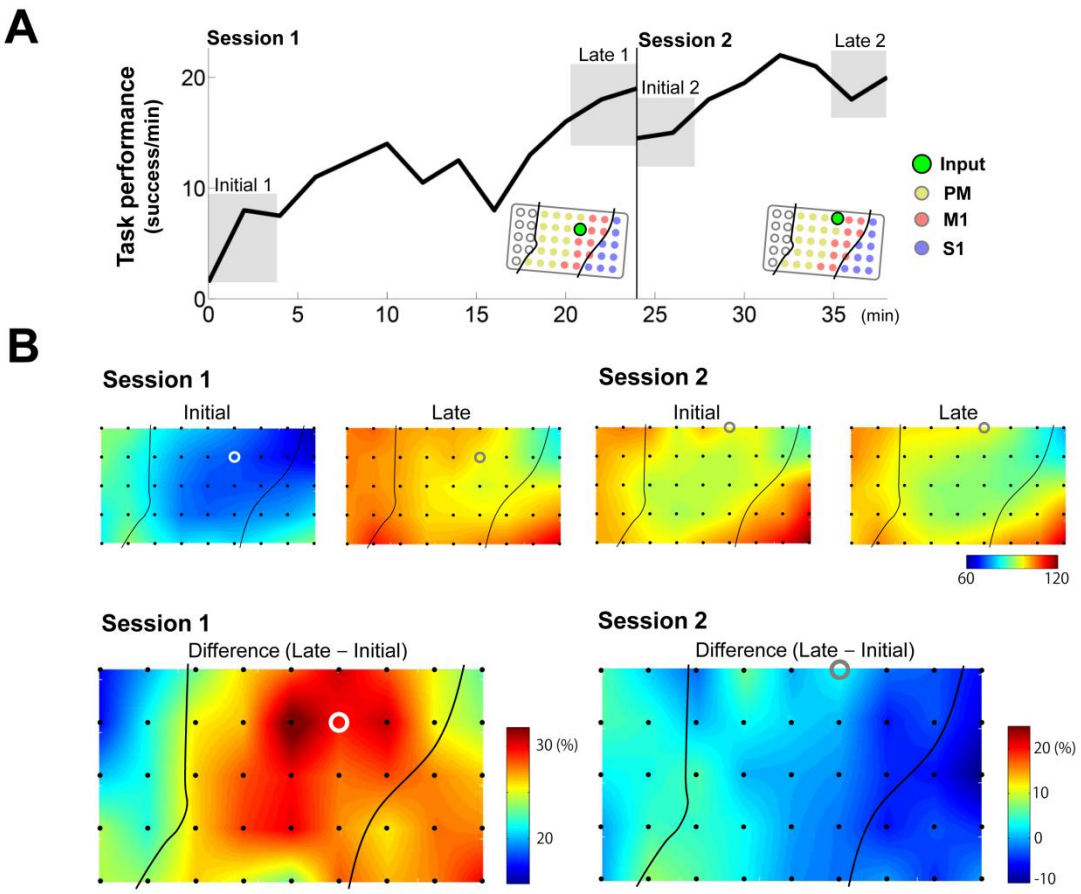
A
Session 1
Session 2
Late 1
Late 2
Initial 2
Initial 1
Task performance
(success/min)
20
10
0
0
5
10
15
20
25
30
35
(min)
Input
PM
M1
S1
B
Session 1
Initial
Late
Session 2
Initial
Late
60
120
Session 1
Difference (Late – Initial)
30 (%)
20
Session 2
Difference (Late – Initial)
20 (%)
10
0
-10

Fig. 12

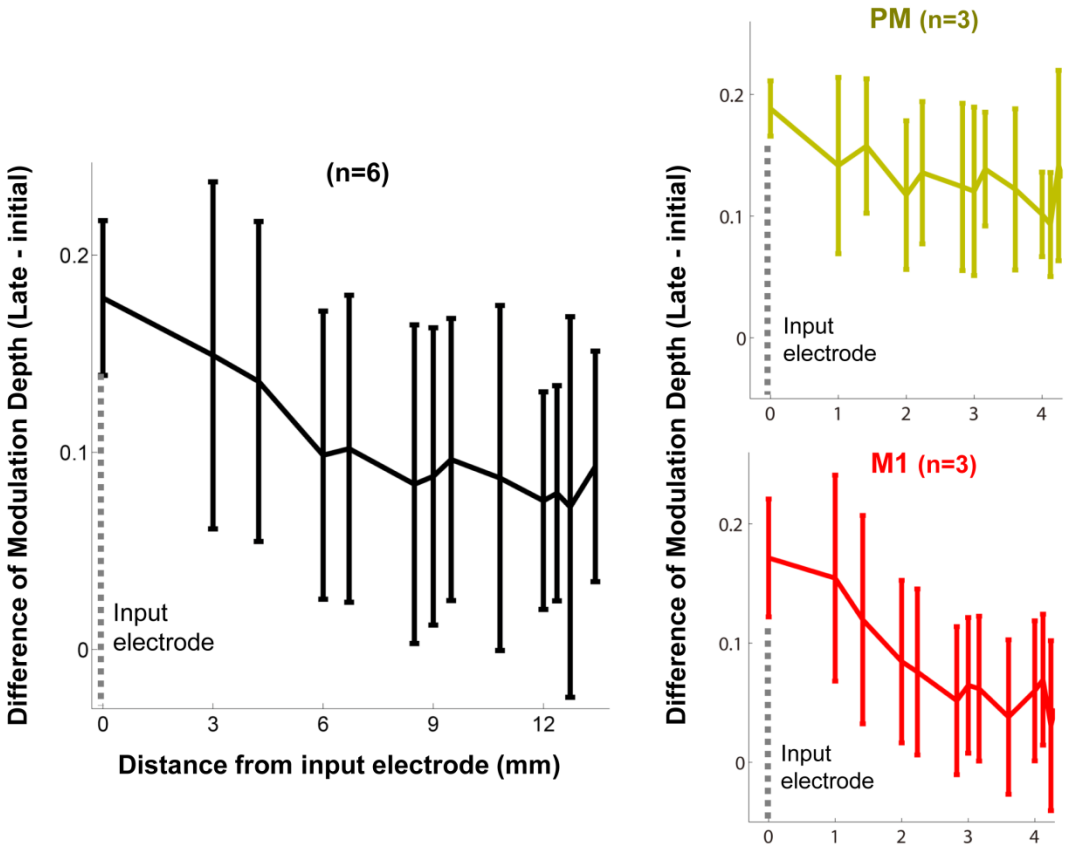
(n=6)
Difference of Modulation Depth (Late - initial)
0.2
0.1
0
Input
electrode
0
3
6
9
12
Distance from input electrode (mm)
PM (n=3)
0.2
0.1
0
Input
electrode
0
1
2
3
4
M1 (n=3)
0.2
0.1
0
Input
electrode
0
1
2
3
4

Part II

Title: Flexible Adaptation to an Artificial Recurrent Connection from Muscle to Peripheral Nerve in Men

Abstract

Controlling neuroprotheses such muscle-controlled external devices or functional electrical stimulation requires leaning a novel input-output transformation, however how to incorporate it remains obscure. To investigate underling mechanisms, we investigated the motor adaptation process to a novel artificial recurrent connection from a muscle to peripheral nerve (ARC) in humans. This paradigm stimulated the ulnar nerve for homonymous muscle in proportion to activation of homonymous or synergist muscle and induced boosting the on-going activity of homonymous muscle and wrist movement during the visually-guided reaching task about wrist. We found that participants could learn to utilize a novel ARC into the volitional control of wrist movement, and re-adapt to without the ARC in either case. Participants had significantly reduced homonymous muscle recruitment with practice regardless of the input muscle to ARC. However adaptation process in synergist muscle was depending upon the input muscle; the activity of synergist muscle decreased when the input was the homonymous muscle whereas increased when it was the synergist muscle. Furthermore, this reorganization of neuromotor map maintained as after-effect of the ARC was observed only when input was the synergist muscle. These findings demonstrate that neuromotor map was reorganized and recalibrated in a targeted and

sustainable manner through the ARC. This protocol may develop for a potential neuroprosthetic treatment for individuals who have residual neural systems after damage in descending motor pathways.

Keywords: motor adaptation, artificial neural connection, volitional control, brain-computer interface

Introduction

It is estimated that, over five million and 130,000 worldwide people each year suffer from stroke (http://www.world-heart-federation.org/cardiovascular-health/stroke/, 2013) and a spinal cord injury (SCI, http://www.campaignforcure.org, 2011) that are permanently disabled. Such neural damage often leads to partial paralysis and impairs ability to execute daily activities on their own even if their residual neural circuits remained functional.

Realistic solutions to restore lost function are the use of a functional electrical stimulation (FES) in paretic muscle and orthotic exoskeleton. The orthotic exoskeleton thought to be profit to individuals with amputees, whereas FES would be a better choice for individuals with SCI or stroke whose extremities remains functional. In typical systems of FES, the patient uses switches (Vodovnik et al., 1965, Brandell, 1982, Burridge et al., 1997, Liberson et al., 1961, Waters et al., 1975), or muscle activity (Peckham et al., 2001; Popovic et al., 2001; Frigo et al., 2000; Muraoka, 2002; O'Keeffe and Lyons, 2002) to trigger pre-programmed patterned stimulation of paralyzed muscles to produce stereo-typed movements. These produce an all-or-none triggering of FES and are not adaptable for making on-line adjustments. Recent methodological studies have developed closed-loop FES which controls the intensity of

electrical stimulation in proportional into the envelope of electromyography (EMG; Yeom and Chang, 2010). These later methods cleared up problems of uncontrollable behaviors induced by non-volitional, pre-programmed stimulation, and well demonstrated that subjects controlled the closed-loop FES, however, how subjects incorporate it in limb control is still unclear.

Humans adaptively control limb movements to maintain good performance in the presence of novel forces on the limb (Gottlieb, 1994; Shadmehr and Mussa-Ivaldi, 1994, Brashers-Krug et al., 1996; Shadmehr and Brashers-Krug, 1997). It has demonstrated that humans can learn to make reaching movement in novel dynamical environments or force fields. Motor commands that generate reaching movements are constructed by the central nervous system by taking into account predicted force output (Gottlieb, 1994; Shadmehr and Mussa-Ivaldi, 1994). With practice, descending motor commands are modified to recalibrate new neuromotor map which is an association between a desired limb movement and the corresponding motor commands.

In the current study, I investigated the motor adaptation process to a novel closed-loop FES, which is an artificial recurrent connection from a muscle to peripheral nerve (ARC). The ARC was accomplished by a computer interface which was designed to detect the firing pattern of a putative motor unit and converted in real-time to

activity-contingent electrical stimuli delivered to the peripheral nerve to boosting activity of homonymous muscle, so that subjects could voluntarily alter of electrical stimuli to the peripheral nerve. I focused on goal-directed wrist movement and measured the task performance and muscle activities to understand neuronal mechanisms of the motor adaptation process in a novel artificial connection.

Methods

Participants

Twenty-two healthy right-handed volunteers (age range 25-43, mean±SD: 32.5±5.6 years, 1 females) were participated in the experiments, which was consisted of three types of the experiments; “Pre-Experiment 1”, “Pre-Experiment 2”, and “ARC Experiment” see below in details. In ARC Experiment, varying subgroups of participants performed in the three different conditions, “Control”, “ARC with Homonymous” and “ARC with Synergist” see below in details. Some participants performed more than one experiment. In this case, the interval between successive experimental sessions was at least 8 weeks to avoid carryover effects. None of the participants had a history of neurological disease at the time of the experiments. Written informed consent was obtained before participation. The experiments conformed to the Declaration of Helsinki and were approved in advance by the ethics committee of the National Institute for Physiological Sciences, Okazaki, Japan (Approved No. 12B009).

Experimental Setup

Participants sat on a chair while grasping the handle of a robotic manipulandum (Phantom Premium 1.5 High Force, SensAble Technologies) with their

right hand (**Fig. 13A**). The manipulandum measured position and torque in flexion-extension (F-E) and radial-ulnar (R-U) directions produced about the wrist. A spring force field (0.07 N/cm) was generated in a vertical plane. The right forearm was immobilized in a horizontal plane approximately parallel to the ground by the custom-built fixture. The shoulder abducted at 45°, the elbow was kept at 110°, and the wrist joint in neutral position at 0° and could move their wrist joints freely during the task. The monitor positioned at eye level to display the position of the handle with a blue square cursor (size 8 mm) on a vertical screen.

Recordings

Electromyographic (EMG) activity was recorded with bipolar surface electrodes (NM-512G, Nihonkoden, Tokyo, Japan) placed on muscle bellies of flexor carpi ulnaris (FCU), palmaris longus (PL), flexor carpi radialis (FCR), extensor carpi radialis (ECR), and extensor carpi ulnaris (ECU) on right arm. EMG signals were amplified (×1000, MEG-6116; NIHON KOHDEN, Tokyo, Japan) and band-pass filtered at 50–3000 Hz. EMG signals were converted into digital data via an A/D converter system at a sampling rate of 5 kHz for later off-line analysis (CED 1401 interface with Spike2 software; CED, Cambridge, UK). The position, torque signals in F-E and R-U

directions from a robotic manipulandum were simultaneously recorded at a sampling rate of 5 kHz, and were down-sampled to 1k Hz for off-line analysis.

Ulnar nerve electrical stimulation

Electrical stimuli were delivered to the ulnar nerve at the elbow level via surface electrodes in trains of 1 ms duration biphasic square-wave pulses (FHC, Bp Isolator, Bowdoin, USA). A pair of electrodes for the ulnar nerve stimulation was placed on the medial surface of the elbow, just proximal to the medial epicondyle of humeral (**Fig. 13A**). The ulnar nerve was identified by confirming the evoked responses of the ulnar-innervated muscles, which is homonymous muscle (FCU), gradually increasing the stimulus current at 1 Hz at rest. The motor threshold (MT) was defined as the minimal current at which the evoked muscle twitch was observed. The participants confirmed that the electrical stimulus was not painful.

Experimental Paradigms

Each participant was instructed to perform the visually-guided reaching task about wrist. Visual feedback was provided by cursor represensting the position of the manipulandum handle on computer screen (**Fig. 13A**). The center of the cursor

corresponded to the position of the wrist joint at rest. In the behavioral paradigm, the center target (size 4.2 cm) first appeared and subjects were relaxed and holding in the center target for 1 sec. After holding the center target, a peripheral target (size 3.1 cm) appeared, and participants were required to move the cursor into the peripheral target. After holding the peripheral target for 1 sec, participants were required to go back to the center target. Each participant performs the center-out task in three different conditions: the task without electrical stimulation (Pre-Experiment 1), with a continuous electrical stimulation (Pre- Experiment 2), and with ARC from a muscle to peripheral nerve (ARC Experiment).

Pre-Experiment 1

The participants performed the center-out reaching task to randomly-selected targets from the 8 radial positions (45° apart) without stimulation to confirm the directional tuning of the muscle activity. A peripheral target appeared randomly from the eight locations evenly spaced in a corresponding to 6 cm of actual distance in center-out movement. The participants continued to perform the center-out reaching task at least 30 times in each of peripheral targets. .

Pre-Experiment 2

Next, the participants performed the center-out reaching task to the 8 radial positions with the continuous electrical stimuli to the ulnar nerve with the current at MT×1.1 and frequency at 3 Hz. This task was used to confirm the direction of the evoked wrist movement and muscle responses those were induced by the ulnar nerve electrical stimuli. The participants continued to perform the center-out reaching task at least 30 times in each of peripheral targets.

ARC Experiment

Lastly, the participants performed the reaching task to a target in three different epochs, denoted as “baseline” without ARC, “ARC” with ARC, and “Washout” without ARC. Immediately following baseline epoch during 420 trials (trials: 1-420), the participants began ARC epoch without any instruction to the participants during which they performed 420 trials with the ARC (trials: 421-840). Immediately after “ARC” epoch, ARC was terminated, and participants then performed 140 movements without ARC as “Washout” epoch (trials: 841-980). The location of a target was set at the same location with the end-point while the 50 Hz continuous electrical stimuli with MT×1.3 applied to the ulnar nerve. The actual distance between center and peripheral target was

set in 5.5-6.0 cm averaged the subjects.

Artificial recurrent connection

An artificial recurrent connection (ARC) was accomplished by a computer interface which was designed to detect the firing pattern of a putative motor unit which shows similar waveforms and converted in real-time to activity-contingent electrical stimuli delivered to the ulnar nerve (**Fig. 13**). The firing pattern of putative motor units controls both stimulation current and frequency in proportional to the moving averaged firing frequencies (250 ms time window) of the particular muscle activities, so that subjects could voluntarily alter both the current and frequency of electrical stimuli to the ulnar nerve. If the firing frequencies of the particular EMG waveforms (X [Hz]) was above stimulus threshold (X_{th} [Hz]), stimulus frequency (f [Hz]) and current (I [mA]) were modulated by the equations as follows;

$$f = f_0 + \frac{f_g}{X_{th}} \cdot X, (f_0 \leq f \leq f_{Max}) \qquad \text{eq.1}$$

(f_0 = the initial stimulus frequency when X [Hz] was above X_{th} [Hz], f_g = the gain of stimulus frequency, f_{Max} = maximum stimulus frequency [Hz])

$$I = I_0 + \frac{I_g}{X_{th}} \cdot X, (I_0 \leq I \leq I_{Max}) \qquad \text{eq.2}$$

(I_0 = the initial stimulus current, I_g = gain of stimulus current, I_{Max} = maximum

stimulus current [mA])

Across the subjects, these parameters ranged as follows; (X_{th}: 0.3-0.5 Hz, f_0: 20-30 Hz, f_g: 0.3-0.5 Hz, f_{Max}: 50 Hz in all subjects, I_0: MT×1.0-1.1, I_g: 0.05-0.08 mA, I_{Max}: MT×1.4-1.6).

The participants were randomly assigned to three experimental groups, “Control”, “ARC with Homonymous” and “ARC with Synergist”. In this study, a muscle from the recorded muscles was chosen as the input muscles, which were converted to activity-contingent electrical stimuli to the ulnar nerve. One was the FCU muscle, the innervated muscle of the ulnar nerve, defined as “homonymous” muscle. The PL muscle, which tuned similar direction with homonymous muscle, however, the PL muscle was not innervated by the ulnar nerve, defined as “synergist” muscle. Therefore, each subject could boost the on-going muscle activities of homonymous muscle by ulnar nerve electrical stimuli controlled by the input muscle of homonymous or synergist muscle. The ARC from homonymous muscle to the ulnar nerve (ARC with homonymous) was performed in 10 subjects, and the ARC from synergist muscle to the ulnar nerve (ARC with synergist) was performed in 11 subjects. In control experiment, the 10 subjects performed center-out task continuously without ARC during baseline, ARC, and washout epoch (Control)

Evaluation of the muscle activity

In order to investigate the descending motor commands to motoneuron pools, I measured the rectified EMGs during the holding phase to the peripheral target in each trial. However, in ARC epoch, the artifacts of the electrical stimulation are superimposed with the raw EMG signals. Therefore, I set the "catch trials" during late ARC epoch, in which the ARC suddenly terminated while the subjects were holding in the peripheral target. The recorded muscle activities from 50 ms to 150 ms just after the catch trials were used to measure the muscle activities during the late ARC epoch (trials: 741-840). The 10 catch trials were performed in each subject without any instruction to the subject. The muscle activities were normalized on the basis of the averaged muscle activities in the last 10 trials of baseline epoch, and compared to those in control experiment in which participants performed the same task without ARC. The only difference between ARC experiment (ARC with homonymous or synergist) and control experiment is whether the subject performed to the ARC during ARC epoch. The difference of the recorded muscle activities between ARC and control experiments was evaluated by the unpaired t test.

Results

Relationship between muscle tuning and output effect of ulnar-nerve electrical stimuli

Figure 14B shows the muscle tuning curves while a participant holding the 8 different peripheral targets in Pre-Experiment 1. The averaged preferred direction of Homonymous, Synergist and Antagonist muscles were 192.1±14.8°, 241.8±8,1°, and 323.2±9.4°, respectively. The tuning curves of homonymous and synergist muscle were overlapped and similar with each other (difference between Homonymous and Synergist was 49.8±12.8°), which were tuned to the F-U direction. On the other hand, the tuning curve of antagonist muscle was in E-U direction, which was opposite to that of homonymous muscle (difference between homonymous and antagonist muscle was 131.1±21.4°). In addition, the direction of the evoked movement by electrical stimuli was 229.2±10.3°, which was closest to the preferred direction of Homonymous (difference between evoked movement and Homonymous was 12.6±5.9°).

Figure 14C showed the stimulus triggered averaging of rectified EMGs of the homonymous, synergist, and antagonist muscle during holding the Center and FU targets, and movement phase while performing the center-out task toward FU target with the continuous stimulation. The clear M- and H responses were observed in only

homonymous muscle at all phases whereas no obvious responses were observed in synergist and antagonist muscles. H-response was modulated depending on the task phase due to excitability of motoneuron. Therefore, stimulation on the ulnar nerve induced wrist movement to the particular direction (229.2 $\pm$ 10.3° across the participants) in resting, moving, and holding states.

Artificial recurrent connection from muscle to the ulnar nerve

The ARC was produced by a muscle-computer interface that converts the averaged firing rates of discriminated a putative MU events from the input muscle in real-time into proportional electrical stimuli to the ulnar nerve (**Fig 13**). Homonymous or Synergist was chosen as the input muscle to ARC. **Figure 15** shows the experimental paradigm of the ARC from homonymous (**Fig. 15A**) or synergist (**Fig. 15B**) muscles to the ulnar nerve. The template matching method was employed to discriminate a putative MU (**Fig. 15b**). In both input muscles, the stimulus artifacts have never been contaminated with MU waveform (**Fig. 15c**). Therefore, the participants could control both the stimulation by modulating the firing pattern of a putative MU. The averaging firing frequency of the input putative MU was 0.7±0.6 Hz while the cursor was in the center target and 37.6±13.3 Hz while the cursor was in the peripheral target.

Adaptation to an artificial recurrent connection

In ARC Experiment, each participant performed the task in three sequential epochs: baseline epoch in 420 trials, ARC epoch in 420 trials, and washout epoch in 140 trials. Fig. 16 shows a representative learning process with ARC with Homonymous, showing the hand trajectory, position and velocity profiles on 2D plane for 30 sec in each epoch. During just few trials in early phase in baseline epoch, the cursor have undershot the target, however, the performance have improved in late phase in baseline epoch. After 420 trials in baseline epoch, ARC was suddenly applied without any instruction to participants. ARC boosted on-going muscle activities of homonymous muscle; thereby the wrist trajectories substantially overshot the target in early ARC epoch. The velocity profiles also showed their discrete peaks, which were completely different from that in baseline epoch. The success trials substantially reduced in early ARC epoch (n=4) compared to baseline epoch (n=13). However, as the practice progressed with ARC, the wrist trajectories have hit the target in the late ARC epoch as the performance was significantly increased in late ARC epoch (n=13), which was same level as in baseline epoch. This indicated that the participant could learn to control volitionally ARC, which boosted the on-going muscle activity of homonymous muscle. After 420 trials were

completed with ARC, ARC were suddenly terminated without any instruction to the subject, the cursor undershot the target in just 10 trials during washout epoch. Trial by trial, the participant gradually turned back to the kinematic pattern that was similar to that in baseline epoch (**Fig 17**). In late washout epoch, the performance has completely been the same as that in baseline epoch.

To quantify the performance of each trial over the three epochs across the participants, I measured the overshot distance from the peripheral target in each trial. The averaged overshot distances in ARC with homonymous and synergist muscle were shown in **Figure 18Aa** and **Ba**. The overshot distance in both conditions was around zero in baseline epoch. However, the value of the overshot distance was the maximum in the first trial of the ARC phase, suggesting the ARC boosted the on-going muscle activity of homonymous muscle. However, the overshot distance gradually reduced trial by trial, which was evidenced by the clear learning curves over 420 trials in ARC epoch. A repeated-measures ANOVA found that the reduction in the overshot distance was reliable for both ARC patterns ($p<0.005$ in each case). This suggested that participants could learn to control their movements with the ARC, and the adaptation process in ARC with homonymous muscle was similar with that in ARC with Synergist. However, convergence point of the overshot distance was longer in ARC with synergist muscle

than in ARC with homonymous muscle, suggesting that controlling ARC with synergist was more difficult than ARC with homonymous muscle.

To investigate the further details of the movement patterns in each trial, I calculated the maximum velocity distance which is the distance from the center target to the point where the velocity of movement was highest in each trial, showing figure **18Ab** and **Bb**. Interestingly, in the first trial in the washout phase, the maximum velocity distance was lowest all epochs, which indicated that the cursor undershot the target. However, the maximum velocity distance was quickly turned back to the values in the control phase. These velocity patterns were similar between ARC with homonymous and ARC with synergist.

Neuronal mechanism of adaptation to an artificial recurrent connection

To investigate the neuronal mechanism of this adaptation to the ARC, I measured the muscle activities during hold phase thought the sessions (**Figure 19**). In baseline epoch, the activity of homonymous muscle gradually increased among 300 trials, whereas the activity of synergist muscle gradually decreased. But these changing plateaued after 300 trials. In ARC epoch, since the artifacts of the electrical stimuli interfered with evaluation of muscle activity, I set “catch trials” during late ARC epoch,

in which the ARC suddenly terminated while participants were holding in the peripheral target. In ARC with homonymous, the resultant activities of both homonymous and synergist muscles in “catch trials” significantly decreased compared to those in baseline experiment (p<0.01 in Homonymous, p<0.05 in Synergist). On the other hand, in ARC with synergist, the activity of synergist which was the input muscle to ARC increased (p<0.01) while the activity of homonymous muscle decreased (p<0.005).

I further analyzed the muscle activities in the washout epoch. Interestingly, in only with synergist, the after-effect of the ARC could be observed in homonymous and synergist muscle. The activities of homonymous muscle substantially decreased over 40 trials, compared to that in control experiment (p<0.00001: 1-10th, p<0.005: 11-20th, p<0.05: 21-40th), and returned to the same level with the control experiment after 40 trials of washout epoch. On the other hand, the activities of synergist muscle continued to increase until 80 trials in the washout epoch (p<0.005: 1-40th, p<0.05: 41-80th). As for ARC with homonymous, there was not significantly change in all muscles.

Discussion

Here I demonstrated that participants were able to learn to utilize a novel recurrent connection from a muscle to peripheral nerve into the volitional control of hand. However, adaptation process was depending upon the input muscle; the descending inputs to synergist muscle decreased in ARC with homonymous muscle whereas increased in ARC with synergist muscle. In particular, in ARC with synergist muscle, reorganization of descending command to spinal motoneuron pool occurred and maintain for up to 80 trials, suggesting that ARC could input-selectively induce reorganization and recalibration of neuro-motor map in a sustainable manner.

Muscle-Controlled, Closed-Loop FES to Peripheral Nerve

The development of FES to muscle has sought to restore voluntary limb function. EMG-controlled FES that measures EMG from a muscle to stimulate the residual nervous systems such as affected muscle (Peckham et al., 2001; Popovic et al., 2001; Popovic et al., 2004; O'Keeffe and Lyons, 2002) or spinal cord (Nishimura et al., 2013a). Recent studies have developed closed-loop FES which control the intensity of electrical stimulation in proportional into the envelope of EMG (Yeom and Chang, 2010) using the fixed comb filters (Frigo et al., 2000) or the novel Gram–Schmidt

filtering algorithm, which enabled to digitally cancel residual stimulation artefacts in real-time (Yeom and Chang, 2010). On the other hand, direct cortical controlled FES demonstrated that monkeys could use cortical activity to control FES (Moritz et al., 2008; Pohlmeyer et al., 2009; Ethier et al., 2012). Their paradigm stimulated muscles in proportion to firing frequency of the cortical cell spikes instead of muscle activity. I took similar approach with them, used discriminated muscle activity instead of cell spikes. The wave form of a putative MU were discriminated from surface EMG signal, then firing pattern of a putative MU was used to control stimulation intensity and frequency in proportional to its firing rate. The input signal was extracted by discriminating in real-time a putative MU from surface EMG, which may reflect the single and/or a few motor units. In any case, the firing rate of a putative MU was clearly modulated during the task (**Fig. 13**), thereby the participants could volitionally control the stimulus patterns. Our study demonstrated that template-matching method could also clearly discriminate the putative MU from the residual stimulus artefacts and evoked muscle response such H and M responses (**Fig. 15**). Although firing rate of the discriminated putative MU was slightly higher than a physiological firing rate of a single MU (De Luca et al. 1982; Bigland-Richies 1992). The surface EMG signal contains contributions from a greater number of motor units, thus the discriminated

putative MU would include a few MUs.

Importantly, the degree of the evoked movements was modulated by both the electrical current and frequency. Force output is determined by recruitment and firing rate of MUs. I believe that modulating of both current intensity and frequency is physiologically appropriate way to activate nervous system. It has been shown that motor units are controlled in unison, rather than individually, indicating that they receive a common drive (De Luca et al., 1982; De Luca and Erim, 1994). The common drive received by all the motor units in the pool is translated into individual firing patterns for each motoneuron by the input-output characteristics of the motoneuron (Erim et al. 1996). Therefore, modulating both the stimulus intensity and frequency may enable participants to control their movements more naturally and precisely.

Learning Strategies to ARC

A common implementation of a brain computer interface (BCI) involves decoding the brain activity to control computer cursor (Carmena et al. 2003; Hochberg et al. 2006; Serruya et al. 2002; Taylor et al. 2002) and external devices (Carmena et al., 2003; Velliste et al., 2008; Ganguly et al., 2009; Ganguly et al., 2011; Hochberg et al., 2012). Conceptually, the approach has evolved from experimental paradigms aimed at

elucidating neural coding of normal arm movements (Paninski et al. 2004; Schwartz et al. 1988), with decoding being the inverse of this process. However, BCI control remains slow and inaccurate in comparison to natural movements, with errors corrected only by visual feedback. Considerable improvements are required if these devices are to have real clinical application. An alternative approach is suggested by operant conditioning of brain activity in which subjects are trained to volitionally modulate brain activity under biofeedback conditions (eg. Fetz 1969; Gage et al. 2006). Biofeedback strategy has used to practice to control FES recently, showing monkeys could learn to use cortical activity to control FES to muscle (Moritz et al., 2008), on spinal cord (Nishimura et al., 2013a) after a brief practices of biofeedback task.

In the current paradigm of ARC, participants completely un-known the causal relationship between input muscle activity and output movement through ARC, however could learn it by experiencing the boosting of their movement through unpredictable additional forces created by ARC. The velocity profile provided the behavioral adaptation process in more details (**Fig. 16**). In baseline epoch, the velocity profile was single bell-shaped distribution which would be largely based on the feed-forward control. However, after exposure to ARC, the velocity profile was completely different, involved with several peaks before entering the target, which

might reflect the error-corrected feedback control. In my paradigm, various types of feedback can be used including visual feed-back through the computer cursor representing the hand position and somatosensory feedback through innate somatosensory and artificially-evoked sensation by ARC. It is clear which types of feed-back information contribute to this adaptation process, however, I could find that the single bell-shaped peaks were regained by further practicing as evidenced by the uniformity velocity peak in late ARC, which was similar with in baseline epoch. This might reflect automatic control with ARC, employed the strategy of feed-forward control. In summary, the learning process of skilled control with ARC may reflect the involvement of transformation from feed-back to feed-forward strategy.

Inducement of Input-Specific Reorganization of Neuro-Motor Map

Notably, I found that reorganization of muscle activities could be selectively induced in ARC with synergist muscle, and sustained during 80 trials after washout epoch, although the undershooting in the behavioral changes could be observed within only few trials. Previous studies have demonstrated that motor learning induced a reorganization of sensory and motor representations in the cortex (Buonomano et al., 1998; Sanes et al., 2000). Acquisition of motor skills could alter the somatotopic map of

limb movements in sensorimotor areas (Nudo et al., 1996a; Kleim et al., 1998), and plastic changes have been implicated with the recovery from disorders such as stroke and spinal cord injury (Nudo et al., 1996b; Raineteau et al., 2001; Cramer et al., 2011). The plastic changes can be strengthened with the use of paired stimulation input pathways in the cerebellum (Ito et al., 1982), hippocampus (Huang et al., 2004) and motor cortex (Baranyi et al., 1981). In contrast with those studies, I induced reorganization of neuro-motor map using putative MU of homonymous or synergist muscle to control stimulation of peripheral nerve. This activity-dependent stimulation could may produce more effective conditioning (Jackson et al., 2006; Rebesco et al., 2010; Lucas and Fetz, 2012, Nishimura et al. 2013b), in light of Hebb's postulate, showing that natural patterns of neuronal firing can lead to input-specific plasticity when paired with appropriate postsynaptic depolarization. Previous experiments with similar paradigm with ANC have demonstrated that stable reorganization of motor output could be induced via ANC between two sites in motor cortex (Jackson et al., 2006), from muscle to motor cortex (Lucas et al., 2013) during free behavior. Recent study further demonstrated that the strength of neural connections between motor cortex and spinal cord could be modified with ANC from corticospinal cells to the spinal cord (Nishimura et al., 2013b). These studies showed changes of reorganization persisted in

some cases for more than one day (Jackson et al., 2006; Lucas et al., 2013; Nishimura et al., 2013b), whareas in our paradigm the reorganization was sustained for up to 80 trials (corresponded to about 15 min). The possible reason might be the difference of duration of conditioning. In our experiments, the training with ARC continued within half an hour, which is much shorter than previous studies (Jackson et al., 2006; Lucas et al., 2013; Nishimura et al., 2013b). It might be possible that more prolonged conditioning could lead to more permanent changes. Another key factor in obtaining long-term effects is prolonged conditioning during volitional movements (Everaert et al., 2010), which could lead to structural changes and can be implemented with the sort of portable recurrent neural interface (Jackson et al., 2006b; Mavoori et al., 2005).

Reorganization of muscle outputs means the changes of the state of excitation of the motoneuron pools, which are affected by various descending motor systems including the corticospinal, robrospinal, vestibulospinal, and retinculospinal pathways (Lemon, 2008) as well as spinal reflex pathways and muscle afferents (komori et al, 1992). Further study will allow us to understand which levels contribute to the learning the ARC among spinal cord, subcortical, and cortical areas.

In addition, muscle-controlled FES to peripheral nerve has the strong advantage that stimuli to peripheral nerve can simultaneously facilitate both the motor

and sensory nerves. If subjects can utilize the artificial sensation evoked by peripheral nerve stimuli, this protocol may develop for a potential neuroprosthtic treatment toward the bidirectional restoration of motor and somatosensory functions for individuals with damaged motor or sensory pathways (Vato et al., 2012).

A novel divergence from these approaches would be the application of closed-loop recurrent stimulation controlled by peripheral physiological signals. Employment of muscle controlled recurrent stimulation offers the potential advantage of a robust signal-to-noise ratio and not requiring stable chronic neural recordings. Some invasively recorded brain signals have been used as control signals for external devices such as a robotic arm or computer cursor (Kennedy et al., 2000; Wessberg et al., 2000; Carmena et al., 2003). Instead of relying on invasively recorded cortical signals, I used muscle activity as a surrogate of cortical activity. The volitionally controlled muscle activities are more robust compared to brain activities, such as electroencephalogram, cell spikes and local field potentials, and are easy to record. They must substantially expand the sources of control signals for closed BMIs with wide clinical application (Nishimura et al., 2013a).

In summary, this paper demonstrates that recurrent muscle-computer interface

allowed the participants to adapt to a novel artificial muscle-peripheral pathway. By appropriately modifying the descending motor commands into spinal circuit, participants could incorporate its operation into more normal behavior. Since I used a single signal derived from either homonymous or synergist muscle to control stimulation, the degree of movement control demonstrated here remains limited. Extending this strategy to control more natural and complex movements would require additional input signals and output spinal sites. So far, neural interfaces have controlled mainly robotic arm. An important advancement has been the demonstration of neural interfaces that can directly control the subject's muscles. Such a recurrent muscle-computer interface has obvious potential prosthetic applications in boosting weak biological connections in individual with stroke and spinal cord injury.

Figure legends

Figure 13. Experimental design of an artificial recurrent connection (ARC).

A: The paradigm of the ARC from a muscle to the ulnar nerve. A hand-position controlled cursor (a blue square) and target (a red square) were displayed on a computer monitor. A muscle-controlled electrical stimulation was delivered to the ulnar nerve at elbow level during visually-guided reaching task.

B: Example of the muscle activity controlled electrical stimulation to the ulnar nerve. The waveforms of putative motor units (MU) (2^{nd} trace) were in real-time selected from raw EMG (1^{st} trace) by template matching methods. Electrical stimulation (Stim Wave. on 5^{th} trace) was delivered to the ulnar nerve with frequency and current were proportional to the smoothed selected putative motor unit (MU) events (4^{th} trace) above a stimulation threshold (red dotted line in 4^{th} trace).

Figure 14. Evoked muscle responses and movements.

A: Relative locations of the recorded wrist muscles (FCU, PL, and ECU) and the ulnar nerve. Ulnar nerve (cyan) innervates FCU muscles defined as “Homonymous” (Blue). PL is synergist of FCU as wrist flexor, defined as “Synergist” (Red). ECU is antagonist of FCU as wrist extensor, defined as “Antagonist” (black). These definitions were

evidenced by the results of evoked movements by the ulnar nerve electrical stimuli and tuning curves of muscle activities showing in **figure 14B**.

B: Example of muscle tuning curves obtained by averaging EMGs from 30 trials per target in center-out task toward the 8 radial targets. The polar plot shows the hold-period muscle activity and the preferred direction calculated by vector summation. The summation of the vectors of muscle tuning of Homonymous (blue line), Synergist (red line), and Antagonist (black line) are also represented. The direction of evoked movement by the ulnar nerve stimuli is represented in cyan. Preferred direction of Homonymous was close to evoked movement direction. Dotted circles show the averaged muscle activities while subjects were holding the center target.

C: Evoked muscle responses and wrist movement. The stimulus triggered averaging of the rectified EMGs of Homonymous (blue), Synergist (red), and Antagonist (black) muscles, and the evoked positions (cyan) during the rest in the center target (left), the moving state from center to peripheral targets (middle), and the holding state inside the peripheral targets (right).

Figure 15. An artificial recurrent connection from Homonymous (A) or Synergist (B) muscle to the ulnar nerve.

a: Experimental design of ARC from a muscle to the ulnar nerve.

b: The inter-event time histogram of a putative motor unit. Waveforms for a putative motor unit (N=100) during ARC are inset on histogram.

c: Muscle responses with an ARC (N=100). From top: Homonymous (blue), Synergist (red), and Antagonist (black) muscles. Stimulus triggered time histogram of putative MU events is also shown on bottom, indicating that putative MU events could be completely removed from the artifacts by the electrical stimulation.

Figure 16. Adaptation process in hand trajectory for a representative participant with ARC from Homonymous to the ulnar nerve.

Typical example of the trajectories (**A**), position (**B**), and velocity (**C**) profiles on 2D plane for each 30 sec in early and late phase in baseline, ARC, and washout epochs. In early ARC epoch, hand trajectories substantially overshot the target because ARC has boosted on-going muscle activities of Homonymous. However, in late ARC epoch, the participant learned to hit inside the target by utilizing the ARC with the practice over 420 trials. As contrasted to early washout epoch, just after disconnecting ARC, hand trajectory has undershot from the target, although the performance became to be the same level as baseline epoch in late washout epoch.

Figure 17. Typical example of hand trajectory for a representative participant in early washout epoch.

The example of position (**A**) and velocity (**B**) profiles during 9 trials just after washout. The position and velocity profiles clearly revealed that the cursor undershot the target in the first trial after disconnection, and gradually returned to be the similar profile with baseline epoch over 9 trials.

Figure 18. Population data of the adaptation process to ARC with Homonymous (A) and Synergist (B).

The data were averaged across all participants, and the gray lines represent ±2 SD.

a: Adaptation process in the overshot distance. The red dotted lines in ARC epoch represent the 95 % confident levels of the overshot distance during the baseline epoch. The yellow dotted lines in ARC epoch represent the fitting curves from the averaged overshot distance during ARC epoch, which clearly reveal to convergent within the 95 % confident level over 420 trials in both connection patterns. The black arrows indicate the points at the intersection of red line with yellow line which means overshot distance retuned to baseline level.

b: The maximum velocity distance which is the distance from the center target to the point where the movement velocity was highest. The aftereffect could be observed in few trials after washout epoch, in which the distance at the maximum velocity was lowest among epochs.

Figure 19. Population data of the adaptation process quantified by muscle activities during ARC with Homonymous (A) and ARC with Synergist (B).

The data were averaged across all participants, and the error bars represent ±XX SD. Each plot represents the averaged muscle activities among 10 trials. The averaged muscle activities in control experiment in which subjects performed the task without ARC are shown in grey. *: $p<.05$, **: $p<.01$ with Un-paired t-test.

Fig. 13

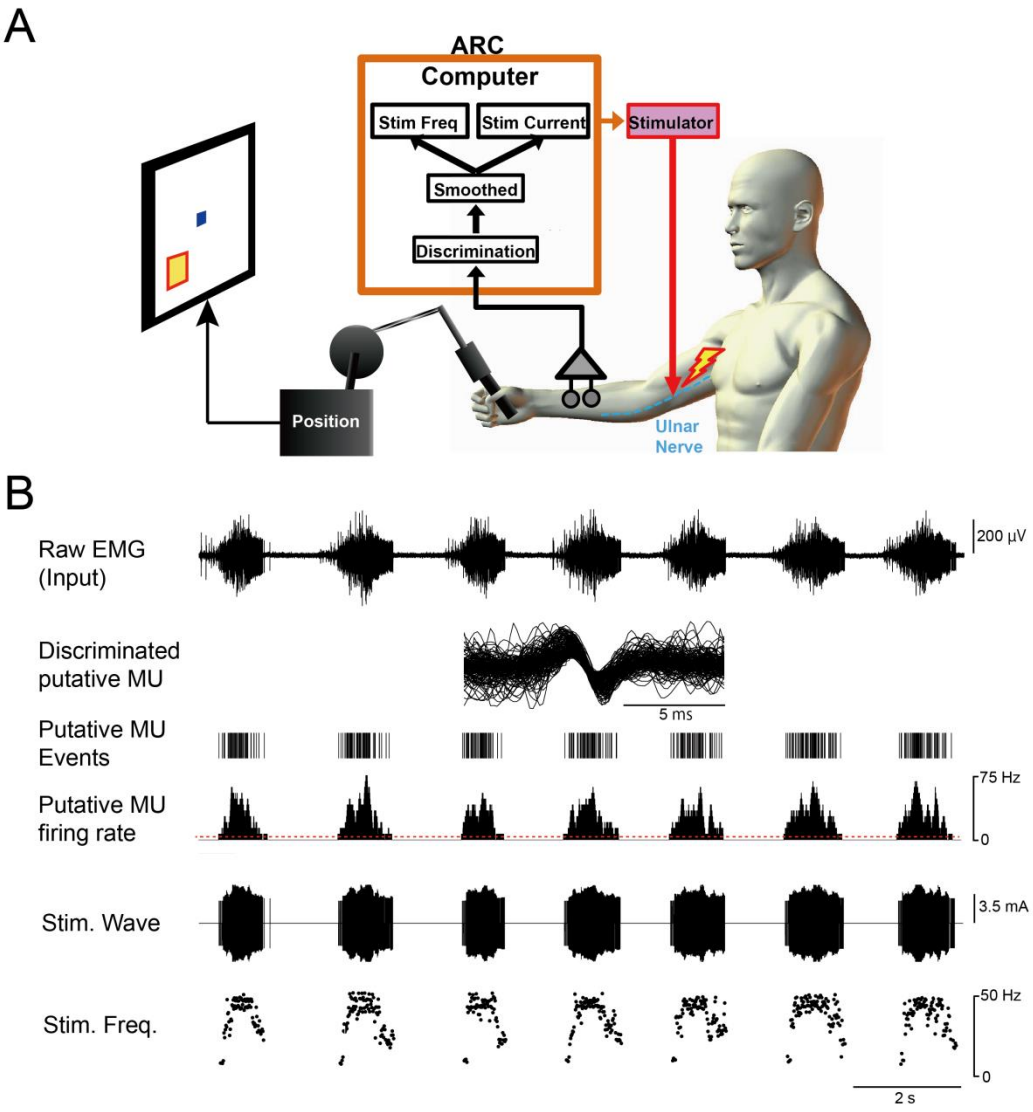
A
ARC
Computer
Stim Freq
Stim Current
Stimulator
Smoothed
Discrimination
Position
Ulnar
Nerve
B
Raw EMG
(Input)
200 µV
Discriminated
putative MU
5 ms
Putative MU
Events
Putative MU
firing rate
75 Hz
0
Stim. Wave
3.5 mA
Stim. Freq.
50 Hz
0
2 s

Fig. 14

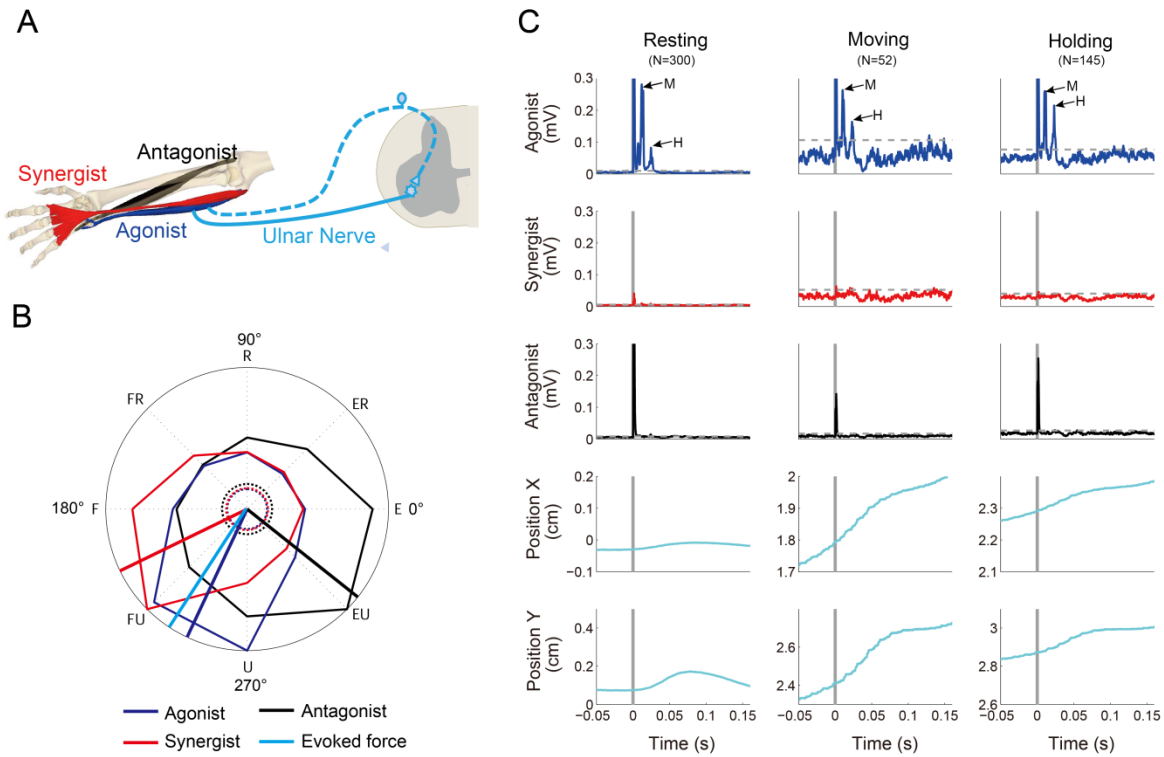
A
Antagonist
Synergist
Agonist
Ulnar Nerve
B
90°
R
FR
ER
180° F
E 0°
FU
EU
U
270°
Agonist
Antagonist
Synergist
Evoked force
C
Resting
(N=300)
Moving
(N=52)
Holding
(N=145)
Agonist (mV)
Synergist (mV)
Antagonist (mV)
Position X (cm)
Position Y (cm)
M
H
Time (s)

Fig. 15

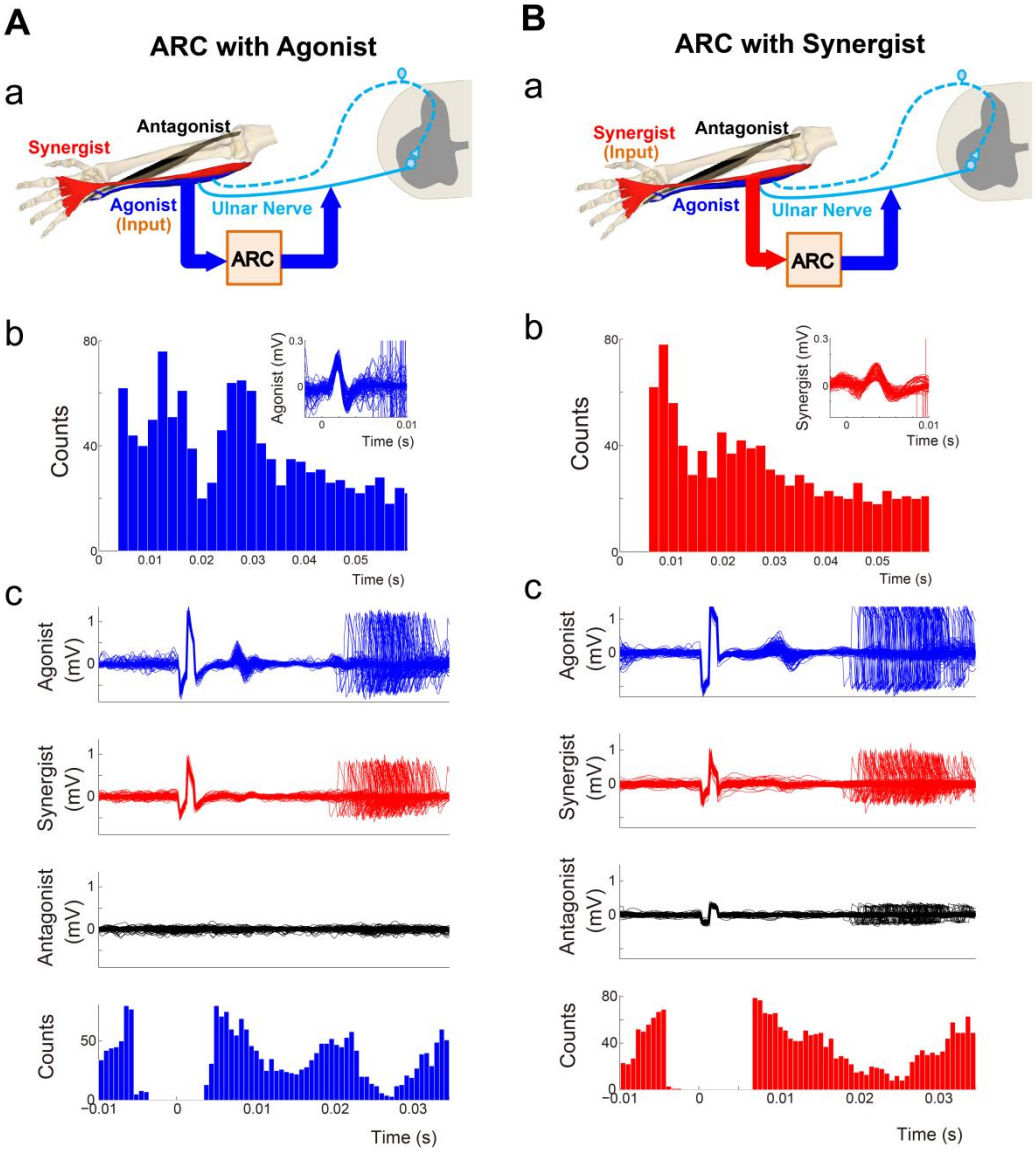
A
ARC with Agonist
a
Antagonist
Synergist
Agonist
(Input)
Ulnar Nerve
ARC
b
Counts
Agonist (mV)
Time (s)
c
Agonist (mV)
Synergist (mV)
Antagonist (mV)
Counts
Time (s)
B
ARC with Synergist
a
Synergist
(Input)
Antagonist
Agonist
Ulnar Nerve
ARC
b
Counts
Synergist (mV)
Time (s)
c
Agonist (mV)
Synergist (mV)
Antagonist (mV)
Counts
Time (s)

Fig. 16

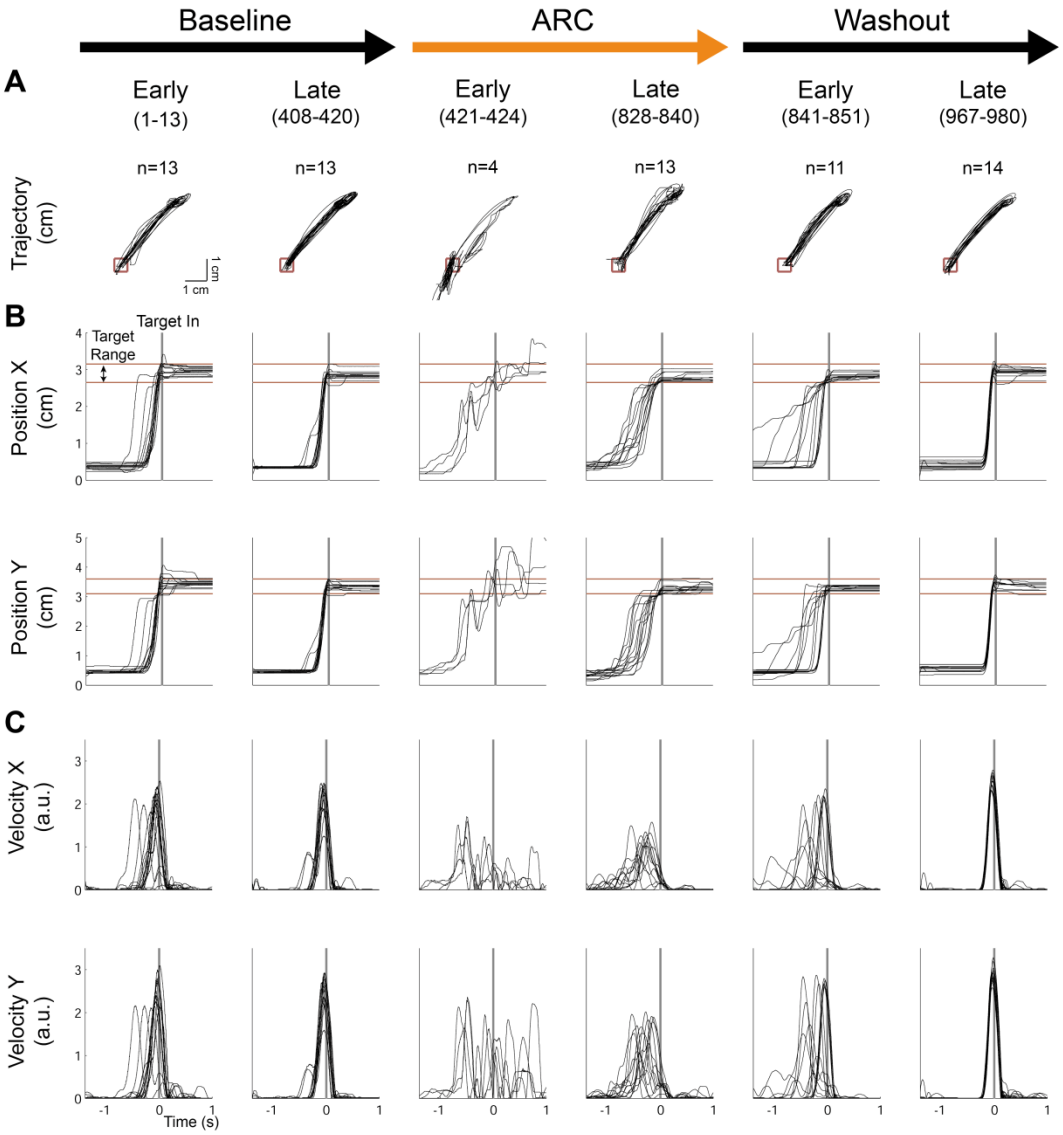
Baseline
ARC
Washout
A
Early (1-13)
Late (408-420)
Early (421-424)
Late (828-840)
Early (841-851)
Late (967-980)
n=13
n=13
n=4
n=13
n=11
n=14
Trajectory (cm)
1 cm
1 cm
B
Target In
Target Range
Position X (cm)
Position Y (cm)
C
Velocity X (a.u.)
Velocity Y (a.u.)
Time (s)

Fig. 17

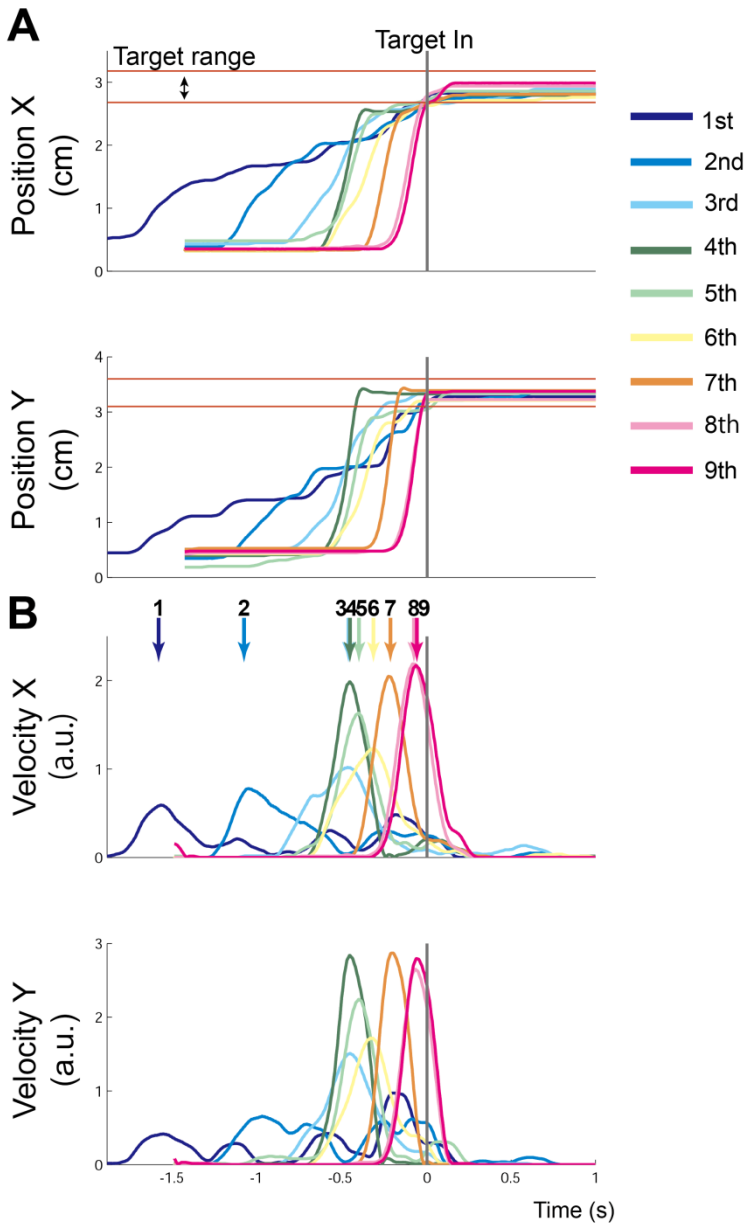
A
Target range
Target In
Position X (cm)
Position Y (cm)
1st
2nd
3rd
4th
5th
6th
7th
8th
9th
B
1
2
3456
7
89
Velocity X (a.u.)
Velocity Y (a.u.)
-1.5
-1
-0.5
0
0.5
1
Time (s)

Fig. 18

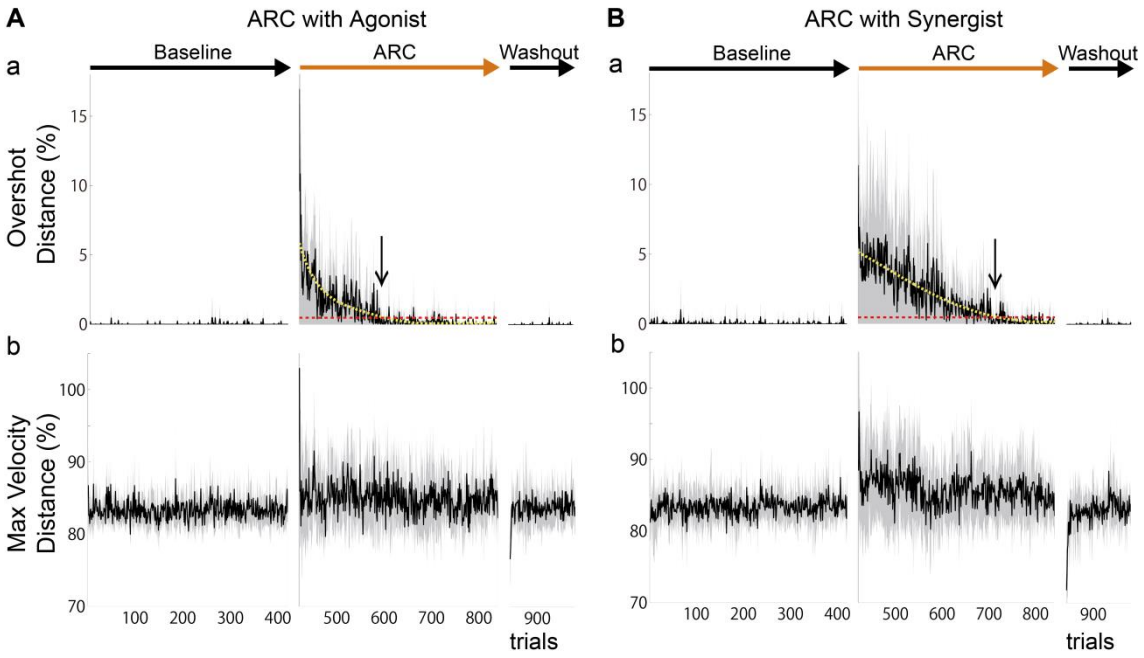
A
ARC with Agonist
Baseline
ARC
Washout
a
Overshot Distance (%)
15
10
5
0
b
Max Velocity Distance (%)
100
90
80
70
100 200 300 400 500 600 700 800 900
trials
B
ARC with Synergist
Baseline
ARC
Washout
a
15
10
5
0
b
100
90
80
70
100 200 300 400 500 600 700 800 900
trials

Fig. 19

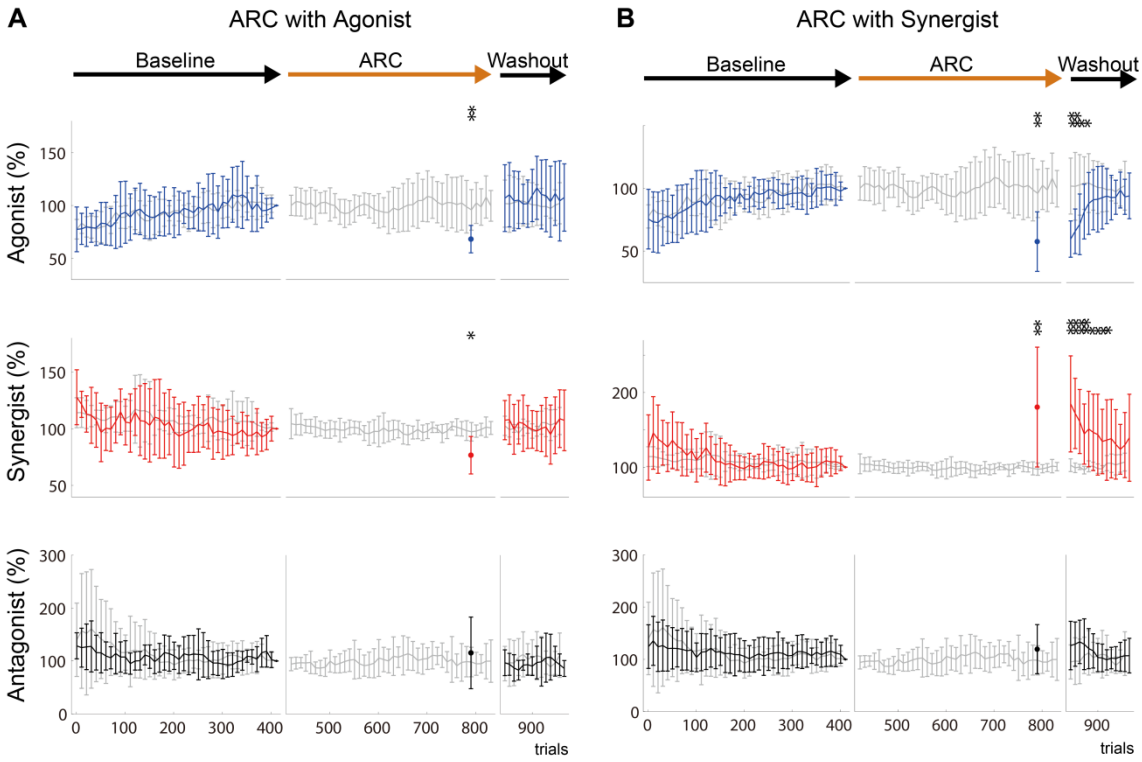
A
ARC with Agonist
Baseline
ARC
Washout
Agonist (%)
Synergist (%)
Antagonist (%)
trials
B
ARC with Synergist
Baseline
ARC
Washout
trials

General discussion

To restore the impaired motor control via an artificial neural connection (ANC), subjects need to learn the input-output causal relationship of ANC, however, the user's adaptability to ANC and neurophysiological mechanism underlying such adaptation process to ANC are still unknown. To answer this, I firstly developed an artificial cortico-muscular connection (ACMC) in monkeys with stroke to restore the goal-directed one-dimensional wrist movements (Part I). By occlusion of the lenticulostriate and anterior coronary arteries, the cerebral peduncle, corona radiata, and putamen were extensively damaged. However, the monkeys still had adequate adaptability to control ACMC. Adaptation to ACMC was rapid, flexible. It was induced by volitionally modulating the firing rates of arbitrarily-selected high-gamma neural oscillations. Secondly, I developed an artificial recurrent connection (ARC) which transforms the muscle activity to stimulate the peripheral nerve, for application of ANC to humans with less invasive approach (Part II). As a result, I found that all the human subjects exhibited adaptability to control ARC by decreasing the descending commands to homonymous muscles.

In this study, an arbitrarily-selected high-gamma cortical activity (Part I), or an arbitrarily-selected muscle activity (Part II) was used as the input signal for controlling

ANC. Importantly, in both studies, the subjects did not know how the input signal affect the actual movement via ANC before exposure to the ANC. Nevertheless, the monkey with stroke as well as human subjects had flexible adaptabilities to control the arbitrarily-assigned high-gamma oscillation recorded from premotor cortex (PM), primary motor cortex (M1), or primary somatosensory cortex (S1), or the arbitrarily-selected muscle activity of homonymous or synergist muscle, by volitionally modulating the input signal.

Previous studies of operant conditioning of neural activity using biofeedback have shown that cells in PM (Nishimura et al., 2013a), M1 (Fetz and Baker, 1973; Fetz and Finocchio, 1975; Moritz et al., 2008; Nishimura et al., 2013a), or S1 (Moritz and Fetz, 2011) with no discernable relation to muscle activity could be volitionally modulated after brief practice sessions. However, a big difference between previous studies and current study was that my paradigm did not set operant conditioning task before ANC session, which might give the opportunity of learning to associate the input signal with a computer cursor to the subject. This suggested that the monkeys with stroke as well as healthy individuals had capacities to learn the causal link between the input signal which was arbitrarily-selected cortical (Part I) or muscle (Part II) activity and output wrist movements through muscle (Part I) or peripheral nerve (Part II)

stimulation, without the experience of associating the input signal with a cursor in pre-operant conditioning task. Therefore, these results could expand the possible range of picking up the controlling signals for brain machine interfaces (BMIs) with wide clinical application.

Another advantage of the protocol in Part I might be to use the thin and flexible structure of the electrocorticographic (ECoG) array, which allowed us long-term stable detection of the cortical signal with low noise (Rubehn et al., 2009). In case of recording with ECoG, modulation of the power of high-gamma band activity could be clearly detected around the onset of movements (Crone et al., 1998; Anderson et al., 2012). Thus, recent studies have shown that ECoG signals in high-gamma frequency range carry rich information sufficient for decoding a set of arm movements (Leuthardt et al., 2004; Mehring et al., 2004; Yanagisawa et al., 2012), and could be appropriate controlling signal for ECoG-based BMIs (Miller et al., 2007, 2008; Yanagisawa et al., 2012; Wander et al., 2013). Notably, we further demonstrated that the ECoG-based closed-loop neural prosthesis could be established in subjects with stroke for restoration of impaired limb functions.

In paradigm of the human study in Part II, we used muscle activity for controlling ANC as a surrogate of cortical activity. Employment of muscle-controlled

recurrent stimulation offers the potential advantage of a robust signal-to-noise ratio which does not require stable chronic neural recordings (Lucas et al., 2013; Nishimura et al., 2013a). In addition, muscle-controlled functional electrical stimulation (FES) to peripheral nerve has the strong advantage that stimuli to peripheral nerve can simultaneously activate both the motor and sensory nerves. If subjects can utilize the artificial sensation evoked by peripheral nerve stimuli, this protocol may develop for a potential neuroprosthtic treatment toward the bidirectional restoration of motor and somatosensory functions for individuals with damaged motor or sensory pathways (Vato et al., 2012).

Reference

1. Anderson, N.R., Blakely, T., Schalk, G., Leuthardt, E.C. & Moran, D.W. Electrocorticographic (ECoG) correlates of human arm movements. *Exp Brain Res* **223**, 1–10 (2012).
2. Badre, D., Kayser, A.S. & D'Esposito, M. Frontal cortex and the discovery of abstract action rules. *Neuron* **66**, 315–326 (2010).
3. Baranyi, A. & Feher, O. Synaptic facilitation requires paired activation of convergent pathways in the neocortex. *Nature* **290**, 413–415 (1981).
4. Bigland-Ritchie, B.R., Furbush, F.H., Gandevia, S.C. & Thomas, C.K. Voluntary discharge frequencies of human motoneurons at different muscle lengths. *Muscle Nerve* **15**, 130–137 (1992).
5. Brandell, B.R. Development of a universal control unit for functional electrical stimulation (FES). *Am J Phys Med* **61**, 279–301 (1982).
6. Brashers-Krug, T., Shadmehr, R. & Bizzi, E. Consolidation in human motor memory. *Nature* **382**, 252–255 (1996).
7. Brinkman, C., Porter, R. & Norman, J. Plasticity of motor behavior in monkeys with crossed forelimb nerves. *Science* **220**, 438–440 (1983).

8. Buonomano, D.V. & Merzenich, M.M. Cortical plasticity: from synapses to maps. *Annu Rev Neurosci* **21**, 149–186 (1998).

9. Burridge, J., Taylor, P., Hagan, S. & Swain, I. Experience of clinical use of the Odstock dropped foot stimulator. *Artif Organs* **21**, 254–260 (1997).

10. Carmena, J.M., Lebedev, M.A., Crist, R.E., O'Doherty, J.E., Santucci, D.M., Dimitrov, D.F., Patil, P.G., Henriquez, C.S. & Nicolelis, M.A. Learning to control a brain-machine interface for reaching and grasping by primates. *PLoS Biol* **1**, E42 (2003).

11. Chapin, J.K., Moxon, K.A., Markowitz, R.S. & Nicolelis, M.A. Real-time control of a robot arm using simultaneously recorded neurons in the motor cortex. *Nat Neurosci* **2**, 664–670 (1999).

12. Cramer, S.C., Sur, M., Dobkin, B.H., O'Brien, C., Sanger, T.D., Trojanowski, J.Q., Rumsey, J.M., Hicks, R., Cameron, J., Chen, D., et al. Harnessing neuroplasticity for clinical applications. *Brain* **134**, 1591–1609 (2011).

13. Crone, N.E., Miglioretti, D.L., Gordon, B. & Lesser, R.P. Functional mapping of human sensorimotor cortex with electrocorticographic spectral analysis. II. Event-related synchronization in the gamma band. *Brain* **121**, 2301–2315 (1998).

14. De Luca, C.J., LeFever, R.S., McCue, M.P. & Xenakis, A.P. Behavior of human motor units in different muscles during linearly-varying contractions. *J Physiol* **329**, 113–128 (1982).

15. De Luca, C.J. & Erim, Z. Common drive of motor units in regulation of muscle force. *Trends Neurosci* **17**, 299–305 (1994).

16. Doya K. Complementary roles of basal ganglia and cerebellum in learning and motor control. *Curr Opin Neurobiol* **10**, 732–739 (2000).

17. Engelhard, B., Ozeri, N., Israel, Z., Bergman, H. & Vaadia, E. Inducing γ oscillations and precise spike synchrony by operant conditioning via brain-machine interface. *Neuron* **77**, 361–75 (2013).

18. Erim, Z., De Luca, C.J., Mineo, K. & Aoki, T. Rank-ordered regulation of motor units. *Muscle Nerve* **5**, 563–573 (1996).

19. Ethier, C., Oby, E.R., Bauman, M.J. & Miller, L.E. Restoration of grasp following paralysis through brain-controlled stimulation of muscles. *Nature* **485**, 368–371 (2012).

20. Everaert, D.G., Thompson, A.K., Chong, S.L. & Stein, R.B. Does functional electrical stimulation for foot drop strengthen corticospinal connections? *Neurorehabil. Neural Repair* **24**, 168–177 (2010).

21. Fabiani, G.E., McFarland, D.J., Wolpaw, J.R. & Pfurtscheller, G. Conversion of EEG activity into cursor movement by a brain-computer interface (BCI). *IEEE Trans Neural Syst Rehab Eng* **12**, 331–338 (2004).

22. Fetz, E.E. Operant conditioning of cortical unit activity. *Science* **163**, 955–958 (1969).

23. Fetz, E.E. & Baker, M.A. Operantly conditioned patterns on precentral unit activity and correlated responses in adjacent cells and contralateral muscles. *J Neurophysiol* **36**, 179–204 (1973).

24. Fetz, E.E. & Finocchio, D.V. Correlations between activity of motor cortex cells and arm muscles during operantly conditioned response patterns. *Exp Brain Res*. **23**, 217–240 (1975).

25. Fincham, J.M. & Anderson, J.R. Distinct roles of the anterior cingulate and prefrontal cortex in the acquisition and performance of a cognitive skill. *Proc. Natl Acad. Sci. USA* **103**, 12941–12946 (2006).

26. Frigo ,C., Ferrarin, M., Frasson, W., Pavan, E. & Thorsen, R. EMG signals detection and processing for on-line control of functional electrical stimulation. *J Electromyogr Kinesiol* **10**, 351–360 (2000).

27. Gandolfo, F., Li, C., Benda, B.J., Schioppa, C.P. & Bizzi, E. Cortical correlates of

learning in monkeys adapting to a new dynamical environment. *Proc Natl Acad Sci USA* **97**, 2259–2263 (2000).

28. Ganguly, K. & Carmena, J.M. Emergence of a stable cortical map for neuroprosthetic control. *PLoS Biol.* **7**, e1000153 (2009).

29. Ganguly, K., Dimitrov, D.F., Wallis, J.D. & Carmena, J.M. Reversible large-scale modification of cortical networks during neuroprosthetic control. *Nat Neurosci* **14**: 662–667 (2011).

30. Georgopoulos, A.P., Taira, M. & Lukashin, A. Cognitive neurophysiology of the motor cortex. *Science* **260**, 47–52 (1993).

31. Gottlieb, G.L. The generation of the efferent command and the importance of joint compliance in fast elbow movements. *Exp Brain Res* **97**, 545–550 (1994).

32. Hikosaka, O., Nakamura, K., Sakai, K. & Nakahara, H. Central mechanisms of motor skill learning. *Curr Opin Neurobiol* **12**, 217–222 (2002).

33. Hochberg, L., Serruya, M.D., Friehs, G.M., Mukand, J., Saleh, M., et al. Neuronal ensemble control of prosthetic devices by a human with tetraplegia. *Nature* **442**, 164–171 (2006).

34. Hochberg, L.R., Bacher, D., Jarosiewicz, B., Masse, N.Y., Simeral, J,D., et al. Reach and grasp by people with tetraplegia using a neurally controlled robotic arm. *Nature*

485, 372–375 (2012).

35. Huang, Y-Y., Pittenger, C. & Kandel, E. R. A form of long-lasting, learning-related synaptic plasticity in the hippocampus induced by heterosynaptic low-frequency pairing. *Proc Natl Acad Sci USA* **101**, 859–864 (2004).
36. International. Campaign for Cures of Spinal Cord Injury Paralysis. http://www.campaignforcure.org (2011).
37. Ito, M. & Kano, M. Long-lasting depression of parallel fibre-Purkinje cell transmission induced by conjunctive stimulation of parallel fibres and climbing fibres in the cerebellar cortex. *Neurosci. Lett* **33**, 253–258 (1982).
38. Ito, M. & Doya, K. Multiple representations and algorithms for reinforcement learning in the cortico-basal ganglia circuit. *Curr Opin Neurobiol* **21**, 368–373 (2011).
39. Izawa, E., Yanagihara, S., Atsumi, T. & Matsushima, T. The role of basal ganglia in reinforcement learning and imprinting in domestic chicks. *Neuroreport* **12**, 1743–1747 (2001).
40. Jackson, A., Mavoori, J. & Fetz, E.E. Long-term motor cortex plasticity induced by an electronic neural implant. *Nature* **444**, 56–60 (2006).

41. Jenkins, I.H., Brooks, D.J., Nixon, P.D., Frackowiak, R.S. & Passingham, R.E. Motor sequence learning: A study with positron emission tomography. *J Neurosci* **14**, 3775–3790 (1994).

42. Kennedy, P.R. & Bakay, R.A. Restoration of neural output from a paralyzed patient by a direct brain connection. *Neuroreport* **9**, 1707–1711 (1998).

43. Kennedy, P.R., Bakay, R.A., Moore, M.M., Adams, K. & Goldwaithe, J. Direct control of a computer from the human central nervous system. *IEEE Trans Rehabil Eng* **8**,198–202 (2002).

44. Kimchi, E.Y. & Laubach, M. Dynamic encoding of action selection by the medial striatum. *J Neurosci* **29**, 3148–3159 (2009).

45. Kleim, J.A., Barbay, S. & Nudo, R.J. Functional reorganization of the rat motor cortex following motor skill learning. *J. Neurophysiol* **80**, 3321–3325 (1998).

46. Komori, T., Watson, B.V. & Brown, W.F. Influence of peripheral afferents on cortical and spinal motoneuron excitability. *Muscle Nerve* **15**, 48 –51 (1992).

47. Koralek, A.C., Jin, X., Long, J.D., 2nd, Costa, R.M. & Carmena, J.M. Corticostriatal plasticity is necessary for learning intentional neuroprosthetic skills. *Nature* **483**, 331–335 (2012).

48. Kuiken, T.A., Dumanian, G.A., Lipschutz, R.D., Miller, L.A. & Stubblefield, K.A.

The use of targetedmuscle reinnervation for improvedmyoelectric prosthesis control in a bilateral shoulder disarticulation amputee. *Prosthet Orthot Int* **28**, 245–253 (2004).

49. Lebedev, M.A., Denton, J.M. & Nelson, R.J. Vibration-entrained and premovement activity in monkey primary somatosensory cortex. *J Neurophysiol* **72**, 1654–1673 (1994).

50. Lemon, R.N. (2008) Descending pathways in motor control. *Annu Rev Neurosci* **31**, 195–218.

51. Leuthardt, E.C., Schalk, G., Wolpaw, J.R., Ojemann, J.G. & Moran, D.W. A brain-computer interface using electrocorticographic signals in humans. *J Neural Eng* **1**, 63–71 (2004).

52. Liberson, W.T., Holmquest, H.J., Scott, D. & Dow, M. Functional electrotherapy in stimulation of the peroneal nerve synchronized with the swing phase of gait in hemiparetic patients. *Arch Phys Med Rehabil* **42**, 101–105 (1961).

53. Lucas, T.H. & Fetz, E.E. Myo-cortical crossed feedback reorganizes primate motor cortex output. *J Neurosci* **33**, 5261–5274 (2013).

54. Mavoori, J., Jackson, A., Diorio, C. & Fetz, E. An autonomous implantable computer for neural recording and stimulation in unrestrained primates. *J. Neurosci Methods* **148**, 71–77 (2005).

55. Miller, K.J., Leuthardt, E.C., Schalk, G., Rao, R.P., Anderson, N.R., Moran, D.W., Miller, J.W. & Ojemann, J.G. Spectral changes in cortical surface potentials during motor movement. *J Neurosci* **27**, 2424–2432 (2007).

56. Miller, K.J., Shenoy, P., den Nijs, M., Sorensen, L.B., Rao, R.N. & Ojemann, J.G. Beyond the gamma band: the role of high-frequency features in movement classification. *IEEE Trans Biomed Eng* **55**, 1634–1637 (2008).

57. Miller, K.J., Schalk, G., Fetz, E.E., den Nijs, M., Ojemann, J.G. & Rao, R.P. Cortical activity during motor execution, motor imagery, and imagery-based online feedback. *Proc Natl Acad Sci USA* **107**, 4430–4435 (2010).

58. Muraoka, Y. Development of an EMG recording device from stimulation electrodes for functional electrical stimulation. *Frontiers Med Biol Eng* **11**, 323–333 (2002).

59. Moritz, C.T., Perlmutter, S.I. & Fetz, E.E. Direct control of paralysed muscles by cortical neurons. *Nature* **456**, 639–642 (2008).

60. Moritz, C.T. & Fetz, E.E. Volitional control of single cortical neurons in a brain-machine interface. *J Neural Eng* **8**, 025017 (2011).

61. Nelson, R.J. Activity of monkey primary somatosensory cortical neurons changes prior to active movement. *Brain Res* **406**, 402–407 (1987).

62. Nicolelis, M.A. & Lebedev, M.A. Principles of neural ensemble physiology underlying the operation of brain-machine interfaces. *Nat. Rev. Neurosci.* **10**, 530–540 (2009).

63. Nishimura, Y., Perlmutter, S.I. & Fetz, E.E. Restoration of upper limb movement via artificial corticospinal and musculospinal connections in a monkey with spinal cord injury. *Front Neural Circuits* **7**, 57 (2013a).

64. Nishimura, Y., Perlmutter, S.I., Eaton, R.W. & Fetz, E.E. Spike-Timing-Dependent Plasticity in Primate Corticospinal Connections Induced during Free Behavior. *Neuron* **80**, 1301–1309 (2013b).

65. Pohlmeyer, E.A., Oby, E.R., Perreault, E.J., Solla, S.A., Kilgore, K.L., Kirsch, R.F. & Miller, L.E. Toward the restoration of hand use to a paralyzed monkey: brain-controlled functional electrical stimulation of forearm muscles. *PLoS One* **4**, e5924 (2009).

66. Nudo, R.J., Milliken, G.W., Jenkins, W.M. & Merzenich, M.M. Use-dependent alterations of movement representations in primary motor cortex of adult squirrel monkeys. *J. Neurosci* **16**, 785–807 (1996a).

67. Nudo, R. J., Wise, B. M., SiFuentes, F. & Milliken, G. W. Neural substrates for the effects of rehabilitative training on motor recovery after ischemic infarct. *Science* **272**, 1791–1794 (1996b).

68. O'Keeffe & Lyons A versatile drop foot stimulator for research applications. *Medical Engineering & Physics* **24**, 237–242 (2002).

69. Peckham, P.H., Keith, M.W., Kilgore, K.L., Grill, J.H., Wuolle, K.S., Thrope, G.B., Gorman, P., Hobby, J., Mulcahey, M.J., Carroll, S., Hentz, V.R. & Wiegner, A. Efficacy of an implanted neuroprosthesis for restoring hand grasp in tetraplegia: a multicenter study. *Arch Phys Med Rehabil* **82**, 1380–1388 (2001).

70. Pohlmeyer, E.A., Oby, E.R., Perreault, E.J., Solla, S.A., Kilgore, K.L., Kirsch, R.F. & Miller, L.E. Toward the restoration of hand use to a paralyzed monkey: brain-controlled functional electrical stimulation of forearm muscles. *PLoS One* **4**, e5924 (2009).

71. Popovic, M.R., Curt, A., Keller, T. & Dietz, V. Functional electrical stimulation for grasping and walking: indications and limitations. *Spinal Cord* **39**, 403–412 (2001).

72. Popovic, D.B., Popovic, M.B., Sinkjaer, T., Stefanovic, A. & Schwirtlich, L. Therapy of paretic arm in hemiplegic subjects augmented with a neural prosthesis: a cross-over study. *Can J Physiol Pharmacol* **82**, 749–756 (2004).

73. Raineteau, O. & Schwab, M.E. Plasticity of motor systems after incomplete spinal cord injury. *Nature Rev. Neurosci* **2**, 263–273 (2001).

74. Rebesco, J.M., Stevenson, I.H., Körding, K.P., Solla, S.A. & Miller, L.E. Rewiring neural interactions by micro-stimulation. *Front Syst Neurosci.* **4** (2010).

75. Rokni, U., Richardson, A.G., Bizzi, E. & Seung, H.S. Motor learning with unstable neural representations. *Neuron* **54**, 653–666 (2007).

76. Sanes, J.N. & Donoghue, J.P. Plasticity and primary motor cortex. *Annu Rev Neurosci* **23**, 393–415 (2000).

77. Schlaug, G., Knorr, U. & Seitz R. Inter-subject variability of cerebral activations in acquiring a motor skill: A study with positron emission tomography. *Exp Brain Res* **98**, 523–534 (1994).

78. Shadmehr, R. & Mussa-Ivaldi, F.A. Adaptive representation of dynamics during learning of a motor task. *J Neurosci* **14**, 3208–3224 (1994).

79. Shadmehr, R. & Brashers-Krug, T. Functional stages in the formation of human long-term motor memory. *J Neurosci* **17**, 409–419 (1997).

80. Soso, M.J. & Fetz, E.E. Responses of identified cells in postcentral cortex of awake monkeys during comparable active and passive joint movements. *J Neurophysiol* **43**, 1090–1110 (1980).

81. Taylor, D.M., Tillery, S.I. & Schwartz, A.B. Direct cortical control of 3D neuroprosthetic devices. *Science* **296**, 1829–1832 (2002).

82. Thach, W.T. Correlation of neural discharge with pattern and force of muscular activity, joint position, and direction of intended next movement in motor cortex and cerebellum. *J Neurophysiol* **41**, 654–676 (1978).

83. Vato, A., Semprini, M., Maggiolini, E., Szymanski, F.D., Fadiga, L., Panzeri, S. & Mussa-Ivaldi, F.A. Shaping the dynamics of a bidirectional neural interface. *PLoS Comput Biol* **8**, e1002578 (2012).

84. Velliste, M., Perel, S., Spalding, M.C., Whitford, A.S. & Schwartz, A.B. Cortical control of a prosthetic arm for self-feeding. *Nature* **453**, 109–1101 (2008).

85. Vodovnik, L., Long, C 2nd., Reswick, J.B., Lippay, A. & Starbuck, D. Myo-electric control of paralyzed muscles. *IEEE Trans Biomed Eng* **12**, 169–172 (1965).

86. Wander, J.D., Blakely, T., Miller, K.J., Weaver, K.E., Johnson, L.A., Olson, J.D., Fetz, E.E. & Rao, R.P. Distributed cortical adaptation during learning of a brain-computer interface task. *Proc Natl Acad Sci USA* **110**, 10818–10823 (2013).

87. Waters, R.L., McNeal, D. & Perry, J. Experimental correction of footdrop by electrical-stimulation of peroneal nerve. *J Bone Joint Surg Am*, **57**, 1047–1054 (1975).

88. Wessberg, J., Stambaugh, C.R., Kralik, J.D., Beck, P.D., Laubach, M., Chapin, J.K., Kim, J., Biggs, S.J., Srinivasan, M.A. & Nicolelis, M.A. Real-time prediction of hand trajectory by ensembles of cortical neurons in primates. *Nature*, **408**, 361–365 (2000).

89. Wise, S.P., Moody, S.L., Blomstrom, K.J. & Mitz, A.R Changes in motor cortical activity during visuomotor adaptation. *Exp Brain Res* **121**, 285–299 (1998).

90. Wolpaw, J.R., McFarland, D.J., Neat, G.W. & Forneris, C.A. An EEG-based brain-computer interface for cursor control. *Electroencephalogr Clin Neurophysiol* **78**, 252–259 (1991).

91. Wolpaw, J.R. & Tennissen, A.M. Activity-dependent spinal cord plasticity in health and disease. *Annu Rev Neurosci* **24**, 807–843 (2001).

92. World Heart Federation., http://www.world-heart-federation.org/cardiovascular-health/stroke/

93. Yeom, H. & Chang, Y.H. Autogenic EMG-controlled functional electrical stimulation for ankle dorsiflexion control. *J Neurosci Methods* **193**, 118–125 (2010).

94. Yin, H.H., Mulcare, S.P., Hilário, M.R., Clouse, E., Holloway, T., Davis, M.I., Hansson, A.C., Lovinger, D.M. & Costa, R.M. Dynamic reorganization of striatal circuits during the acquisition and consolidation of a skill. *Nat Neurosci* **12**, 333–

341 (2009).

95. Zanos, S., Richardson, A.G., Shupe, L., Miles, F.P. & Fetz, E.E. The Neurochip-2: an autonomous head-fixed computer for recording and stimulating in freely behaving monkeys. *IEEE Trans Neural Syst Rehabil Eng* **19**, 427–435 (2011).

Acknowledgements

The dissertation is a part of the requirements for receiving the doctor's degree, conferred by the Graduate University for Advanced Studies. First, I would like to express my deepest gratitude to Associate Professor Yukio Nishimura and Professor Tadashi Isa, Department of Physiological Sciences, School of Life Science, The Graduate University for Advanced Studies, and Division of Behavioral Development, National Institute for Physiological Sciences, for their critical discussions and encouragements for this research. I also would like to extend deep gratitude to Doctor Syusaku Sasada, Division of Behavioral Development, National Institute for Physiological Sciences, for his assistance of experiments and critical discussions relating to this research, and Doctor Masahiro Sawada, Developmental Physiology, National Institute for Physiological Sciences, and Neurosurgery, Kyoto University Medical School of Medicine, for his assistance of surgeries and experiments and discussions relating to this research. I also would like to extend deep gratitude to Nobuaki Takahashi, Division of Behavioral Development, National Institute for Physiological Sciences, for his assistance of surgeries and experiments, and Morio Togawa, Division of Behavioral Development, National Institute for Physiological Sciences, for his technical assistance. Finally, I would like to thank all members of Isa

laboratory; Masatoshi Yoshida, Masaaki Ogawa, Hidenori Watanabe, Rikako Kato, Masatoshi Kasai, Norihiko Takakuwa, Michiaki Suzuki, Yoko Nishihara, Takamichi Toyama, Richard Veale, Kaoru Isa, Kazuko Takada, Yumi Yamanishi, Kotomi Shimizu, Ayumi Shibata, and Yu Shimada for the encouragement for this research.